Journal of Nuclear Medicine, published on April 13, 2018 as doi:10.2967/jnumed.117.205088

Radioiodinated Small Molecule Tyrosine Kinase Inhibitor for HER2 Selective SPECT Imaging

Longguang Tang[1,2#], Chenyu Peng[1#], Bowen Tang[3], Zijing Li[1]*, Xiangyu Wang[1], Jindian Li[1], Fei Gao[1], Lumei Huang[1], Duo Xu[1], Pu Zhang[1], Rongqiang Zhuang[1], Xinhui Su[4], Xiaoyuan Chen[2] and Xianzhong Zhang[1]*

[1]State Key Laboratory of Molecular Vaccinology and Molecular Diagnostics & Center for Molecular Imaging and Translational Medicine, School of Public Health, Xiamen University, Xiamen 361005, China
[2]Laboratory of Molecular Imaging and Nanomedicine (LOMIN), National Institute of Biomedical Imaging and Bioengineering (NIBIB), National Institutes of Health, Bethesda, Maryland 20892, United States
[3]School of Pharmaceutical Science, Xiamen University, Xiamen 361005, China
[4]Zhongshan Hospital Affiliated of Xiamen University, Xiamen 361004, China.

Running title: HER2 selective radioiodinated TKI
Disclosure of Potential Conflict of Interest: No potential conflict of interest is disclosed.
Word count: 4906
Grant Support: This study was financially supported by the National Key Basic Research Program of China (2014CB744503), National Natural Science Foundation of China (21271030, 81471707), and the Intramural Research Program, National Institute of Biomedical Imaging and Bioengineering, National Institutes of Health (ZIA EB000073).

# **First authors**: These authors contributed equally to this work. Longguang Tang and Chenyu Peng, students, Center for Molecular Imaging and Translational Medicine, State Key Laboratory of Molecular Vaccinology and Molecular Diagnostics, School of Public Health, Xiamen University, Xiang'an South Rd., Xiang'an district, Xiamen 361102, China. E-mail: longguang.tang@nih.gov; pchenyu@foxmail.com. Phone/Fax: +86(592)2880641.

* **Corresponding author:** Xianzhong Zhang, PhD, Professor, E-mail: zhangxzh@xmu.edu.cn; Phone/Fax: +86(592)2880645.
Zijing Li, PhD, Assistant Professor, E-mail: zijing.li@xmu.edu.cn.
Center for Molecular Imaging and Translational Medicine, School of Public Health, Xiamen University, Xiang'an South Rd., Xiang'an district, Xiamen 361102, China.

ABSTRACT

Objectives: One of the most clinically relevant molecular aberrations in breast cancer is the overexpression of human epidermal growth factor receptor type 2 (HER2). We aimed to develop a radiolabeled tyrosine kinase inhibitor (TKI) for HER2 targeted breast cancer imaging. In this study, a radioiodinated analog ($^{125/131}$I-IBA-CP) of the HER2 selective inhibitor CP724,714 was prepared and evaluated in HER2 positive or negative subcutaneous human breast cancer xenografts.

Methods: The CP724,714 analog IBA-CP was synthesized and assayed for its inhibitory activities against HER2 and six other tyrosine kinases. $^{125/131}$I-IBA-CP was prepared using a copper-mediated radioiodination method with enhanced labeling yield and molar activity. *In vitro* biological activities, including specific and nonspecific binding of ^{131}I-IBA-CP to its HER2 kinase target were assessed in different cell lines. *In vivo* microSPECT imaging with ^{125}I-IBA-CP and biodistribution studies were conducted in mice bearing HER2-positive, HER2-negative or epidermal growth factor receptor (EGFR)-positive tumors. Nonradioactive IBA-CP and the EGFR inhibitor erlotinib were employed as blocking agents to investigate the binding specificity and selectivity of **$^{125/1}$**^{31}I-IBA-CP toward HER2 *in vitro* and *in vivo*. Additionally, $^{125/131}$I-ICP was prepared by direct radioiodination of CP724,714 for comparison with $^{125/131}$I-IBA-CP.

Results: IBA-CP displayed good *in vitro* inhibitory activity (IC_{50} = 16 nM) and selectivity for HER2 over six other cancer-related tyrosine kinases. $^{125/131}$I-IBA-CP was prepared in a typical radiochemical yield of about 65% (decay-corrected), radiochemical purity of >98%, and molar activity of 42 GBq/μmol at the end of synthesis. SPECT imaging revealed significantly higher uptake of ^{125}I-IBA-CP than ^{125}I-ICP in the HER2-positive MDA-MB-453 tumor. Uptake in the HER2-negative MCF-7 tumor

was much lower. Binding of ^{125}I-IBA-CP in the MDA-MB-453 tumor was blocked by co-injection with an excess amount of IBA-CP, but not by erlotinib.

Conclusion: The radiolabeled HER2 selective inhibitor $^{125/131}$I-IBA-CP is a promising probe for *in vivo* detection of HER2-positive tumors.

Keywords HER2, tyrosine kinase inhibitor, radioiodinated IBA-CP, breast cancer, small animal SPECT

The human epidermal growth factor 2 (HER2) is a member of the human epidermal growth factor receptor (EGFR) family (*1*), which is overexpressed in 20–30% of breast cancers and in a similar subset of non–small cell lung cancers, gastric cancers, ovarian carcinomas and colon carcinomas (*1*,*2*). HER2 expression status is routinely determined in tumor cells *in vitro* using immunohistofluorescence or fluorescent in situ hybridization method (*3*,*4*). However, verification of disease is usually made by core needle biopsy of an accessible lesion, which not only is invasive but also may not represent the larger tumor mass or other sites of disease (*5*,*6*). Therefore, it is necessary to develop a more accurate and noninvasive method for the evaluation of HER2 expression in tumors throughout the body (*7*).

Radionuclide-based molecular imaging techniques such as positron emission tomography (PET) and single photon emission computed tomography (SPECT) may represent an appropriate tool to obtain real-time, non-invasive and quantitative information about HER2 expression *in vivo* with high sensitivity (*8-12*). So far, a number of radiolabeled HER2-targeted imaging probes have been assessed, including anti-HER2 antibodies (*13-15*) or their fragments (*16*), nanobody (*17*), diabody (*18*), affibody molecules (*19*,*20*) and high-affinity peptide ligands (*21*,*22*). Although most of them have shown high accumulation in tumor tissues, imaging with these large molecule radiotracers has limitations due to the unfavorable receptor binding kinetics compared with their systemic clearance (*23*,*24*). Furthermore, although protein and peptide-based probes can image the extracellular tyrosine kinases, they cannot be used to assess the density and status of the intracellular kinases that are the primary targets of tyrosine kinase inhibitors (TKIs) (*23*). The smaller size and faster clearance of tailored TKI drugs provide a unique opportunity to examine the interaction between the drug and its HER2 target *in vivo* (*25*). However, the development of an optimum radiolabeled TKI imaging probe is challenging because of

the great difficulty in balancing the lipophilicity to provide membrane permeability and in the meanwhile to reduce non-specific binding and hepatobiliary excretion (*26*). So far, no selective small-molecule inhibitor of HER2 has been reported as a nuclear imaging agent (*27*). Gniazdowska et al. undertook the synthesis of technetium-99m labeled lapatinib in hopes of developing a potential SPECT imaging agent for HER2 positive breast cancer (*28*). However, since lapatinib is a HER2 and EGFR dual targeting, not a HER2 selective inhibitor, this kind of radiotracer will not be able to distinguish HER2 and EGFR in tumor cells.

To date, a number of compounds have been developed as HER2 selective TKIs (*29-32*). One of them, CP724,714 (Figure 1), was reported to be a potent inhibitor of HER2 receptor kinase (half maximal inhibitory concentration (IC_{50}) = 10 nM) *in vitro* with 500 to 1000-fold selectivity over EGFR and other related receptor tyrosine kinases (*33*). Further, binding of CP724,714 to the HER2 active site was thought to tolerate structural modifications in its amide region (*34*). Hence, we prepared a novel analog of CP724,714 for radioiodination by replacing the 2-methoxyacetamide moiety with 4-iodobenzamide. Herein we report the synthesis and evaluation of the radioiodinated analog, ^{125}I-IBA-CP, as a potential SPECT imaging probe for *in vivo* detection of HER2 expression in breast cancer. The direct iodination product of CP724,714, ^{125}I-ICP, was also prepared for comparison.

MATERIALS AND METHODS

Preparation of Radiotracers

The chemical structures for CP724,714 and its two radioiodinated analogs, $^{125/131}$I-IBA-CP and $^{125/131}$I-ICP, are shown in **Fig. 1**. The synthetic routes and methods are detailed in Supplemental Fig. 1.

In Vitro Studies

All *in vitro* studies were performed following published procedures, as detailed in the supplemental file.

MicroSPECT Imaging

The experimental procedures with animals were approved by the Xiamen University's Animal Care and Use Committee. SPECT/computed tomography (CT) imaging was performed on Balb/C nude mice bearing MDA-MB-453 or MCF-7 breast cancer xenografts with a nanoScan-SPECT/CT preclinical scanner. Imaging data were acquired at 1, 2, 3 and 4 h after the animals were intravenously injected with 18.5 MBq of ^{125}I-IBA-CP (n = 4/group). Blocking studies were performed in MDA-MB-453 mice (n = 4/group) at 3 h after co-injection of ^{125}I-IBA-CP with IBA-CP (200 μg/mice) or erlotinib (200 μg/mice). SPECT imaging with ^{125}I-ICP (18.5 MBq, i.v.) was also conducted at 1 and 2 h post-injection (p.i.) in mice with MDA-MB-453 xenograft (n = 4/group). Duration of the SPECT/CT imaging sessions was about 30 min each.

Biodistribution

Biodistribution of ^{131}I-IBA-CP in MDA-MB-453, MCF-7 or MDA-MB-468 tumor-bearing female mice was performed after i.v. injection of 0.18 MBq ^{131}I-IBA-CP (n = 4/group). Blocking studies were performed in MDA-MB-453 tumor-bearing mice by co-injection with either IBA-CP (200 μg/mice) or erlotinib (200 μg/mice). Biodistribution study of ^{131}I-ICP in MDA-MB-453 tumor-bearing mice was also conducted for comparison. The mice were sacrificed and dissected at 3 h after injection of the

radioligand. Samples of tumor, blood, liver (without the gallbladder) and other major organs were collected and weighed, and radioactivity in each sample was measured with a well-type γ-counter (2480 Wizard^2, PerkinElmer). The results were expressed as percentage injected activity dose per gram of sample (% ID/g, mean ± standard deviation (SD)).

Statistical Analysis

Statistical analyses were performed using one-way variance tests (ANOVA) followed by post-hoc tests with the SPSS statistical software and the level of significance was set at $P = 0.05$ (*P <0.1, **P <0.05 and ***P <0.01).

RESULTS

Chemistry and Radiochemistry

Synthetic routes for the non-radioactive compound IBA-CP, its radiolabeling precursor, and others are shown in Supplemental Fig. 1. All compounds were obtained in good yield and characterized by detailed spectroscopic analyses (Supplemental Fig. 2 and Supplemental Fig. 3).

At first, radioiodinated IBA-CP was synthesized by a two-step method (Supplemental Fig. 1A). To reduce the radiosynthesis time, an optimized one-step radioiodination approach was developed to generate ^{125}I-IBA-CP or ^{131}I-IBA-CP (Supplemental Fig. 1B) with a radiochemical yield of 65.3 ± 5.2% (n = 6) as measured by high-performance liquid chromatography (HPLC). After purification by HPLC, ^{125}I-IBA-CP was obtained in >98% radiochemical purity (Supplemental Fig. 4) and molar activity of ~ 42 GBq/μmol. The total radiosynthesis time, including HPLC purification, was 80-100 min.

Direct labeling of CP724,714 was carried out using the standard Iodogen method to prepare ^{125}I-ICP or ^{131}I-ICP (Supplemental **Fig. 1C**) in high radiochemical yield of 90.3 ± 5.2% (n = 6) and radiochemical purity of >95% (Supplemental Fig. 4E).

The log P values of ^{125}I-IBA-CP and ^{125}I-ICP were measured at 1.82 ± 0.24 (n = 4) and 2.71 ± 0.21 (n = 4), respectively (Supplemental Table 1), indicating that ^{125}I-IBA-CP is less lipophilic than ^{125}I-ICP.

In Vitro and *In Vivo* Stability Study

^{125}I-IBA-CP was stable in both normal saline and murine plasma at 37 °C, with >96% of intact parent compound after 4 h of incubation (Supplemental Fig. 5). The *in vivo* metabolic stability of ^{131}I-IBA-CP and ^{131}I-ICP were measured by analyzing the radiometabolites in the liver, blood, and urine at different p.i. times. Results from these experiments indicated that ^{131}I-IBA-CP was much more stable than ^{131}I-ICP *in vivo* (Supplemental Fig. 6 & 7). Measurement of thyroid activity uptake in normal mice confirmed that *in vivo* deiodination of ^{131}I-IBA-CP was much less than ^{131}I-ICP (Supplemental Fig. 8). As illustrated in our previous work (*35*,*36*), the radioiodinated compounds obtained by the copper-mediated method showed higher *in vitro* and *in vivo* stability than those by traditional electrophilic labeling methods using oxidizing agents such as Iodogen, which may due to the fact that the copper-mediated method places the iodine in an electron-deficient aromatic ring while direct labeling introduces the iodine into an electron-rich one.

In Vitro Inhibition of HER2 Kinase and Selectivity Assays

CP724,714 and its analog IBA-CP were evaluated as inhibitors of HER2 and EGFR kinases in an

assay of poly-Glu-Tyr phosphorylation by recombinant intracellular domains of the respective kinases, as previously described (*31*). Under the experimental conditions, CP724,714 inhibited the activity of HER2 with an IC_{50} value of 11.3 nM (Supplemental Table 2), consistent with the previously reported result (IC_{50} = 10 nM) (*33*). Similarly, the analog IBA-CP selectively inhibited the kinase activity of HER2 (IC_{50} = 16.5 nM) and was 100-fold less potent (IC_{50} = 2,340 nM) as an inhibitor of EGFR tyrosine kinase (Supplemental Tables 2 and 3). To assess its kinase selectivity, IBA-CP was further evaluated as an inhibitor of five other cancer-related kinases (HER4, FGFR-1, PDGFRβ, VEGFR-2, c-Met), and found to be >1,000-fold less potent than for HER2 (Supplemental Table 3).

Cellular Binding Specificity and Cell Internalization

The HER2 and EGFR protein levels in different breast carcinoma cells were evaluated by western blot (WB) (**Fig. 2A**). HER2 protein was overexpressed in MDA-MB-453 and BT-474 cells, while EGFR protein was overexpressed in MDA-MB-468 cells. More quantitative measurements of HER2 and EGFR expression came from flow cytometry analysis in four different cell lines, showing results similar to those from WB analysis (**Supplemental Fig. 9 and 10**). Competition studies revealed that ^{131}I-IBA-CP binding was displaced by increasing amount of the unlabeled compound IBA-CP, with the IC_{50} value calculated at 19 nM (**Fig. 2C**). Saturation analysis displayed a single class of high-affinity binding sites with a mean equilibrium dissociation constant (K_D) of 18 nM for ^{131}I-IBA-CP in the MDA-MB-453 cell line (**Fig. 2D**). Binding specificity was confirmed using cell lines with different levels of HER2 expression, with ^{131}I-IBA-CP cell uptake values positively correlated with HER2 expression levels. Binding to HER2-negative cells was low and almost the same as that in the blocking groups where 100-

fold excess of nonradioactive compound IBA-CP was added to block the binding of ^{131}I-IBA-CP to HER2 receptors (**Fig. 2B**).

In addition, we performed a WB analysis to determine the levels of HER2 and HER-2 tyrosine phosphorylation, EGFR, and EGFR tyrosine phosphorylation proteins before and after incubation with different concentrations of IBA-CP or CP724,714 to further confirm their HER2-specific inhibitory activity in BT-474 and MD-MB-468 cell lines (Supplemental Fig. 11).

Cell internalization assays were conducted with ^{131}I-IBA-CP and ^{131}I-ICP to compare their intracellular accumulation in MDA-MB-453 cells. Slightly more ^{131}I-ICP was internalized than ^{131}I-IBA-CP (Supplemental Fig. 12), probably due to the less lipophilic nature of IBA-CP (Supplemental Table 1).

SPECT/CT Imaging with ^{125}I-IBA-CP and ^{125}I-ICP

Given the favorable tumor cell retention and HER2 specificity of ^{125}I-IBA-CP *in vitro*, microSPECT/CT imaging was performed in nude mice with subcutaneous MDA-MB-453 and MCF-7 tumors. ^{125}I-IBA-CP was shown to have high liver uptake and clear through both renal and hepatobiliary routes, with tumor accumulation in the HER2-positive group reaching a peak level at 3 h p.i. (**Fig. 3A**). Uptake levels of ^{125}I-IBA-CP in other organs were similar in both groups (**Fig. 3A** and **Fig. 3B**). Peak tumor/muscle activity ratio was significantly higher in MDA-MB-453 (T/M = 3.9, **Fig. 3C**) than MCF-7 tumor (T/M = 1.3, **Fig. 3D**) at 3 h p.i. For ^{125}I-ICP, higher uptake was seen in the liver region, with much less uptake in the tumor (Supplemental Fig. 13A), resulting in peak tumor/muscle activity ratio of 2.3 at 1 h p.i. (Supplemental Fig. 13B).

After imaging, the tumors were excised for analysis of HER2 expression by immunohistofluorescence. Excellent correlation was found between SPECT signal intensity and histopathological measurement (Supplemental Fig. 14)

Blocking Studies with IBA-CP and Erlotinib

The binding specificity and selectivity of ^{125}I-IBA-CP in the MDA-MB-453 tumor were evaluated by blocking experiments with IBA-CP and erlotinib. Co-injection of ^{125}I-IBA-CP with nonradioactive IBA-CP resulted in significantly reduced uptake of radioactivity in the tumor (**Fig. 4A** and **4B**). This blocking effect was further confirmed by immunohistochemistry analysis of available HER2 and phosphorylated HER2, shown in Supplemental Fig. 15. On the other hand, co-injection with the EGFR inhibitor erlotinib had no blocking effect on ^{125}I-IBA-CP uptake in the MDA-MB-453 tumor. Taken together, these results demonstrated the binding specificity and selectivity of ^{125}I-IBA-CP toward HER2.

Biodistribution

Biodistribution of ^{131}I-IBA-CP was studied in mice bearing MDA-MB-453, MCF-7 and MDA-MB-468 (HER2-, EGFR+) tumors, as well as in the MDA-MB-453 tumor group with co-injection of IBA-CP or erlotinib as blocking agent (**Fig. 5**). At 3 h after ^{131}I-IBA-CP injection, activity distribution patterns in normal organs were similar among the groups, with highest uptake values in the liver, intestine, and kidneys (**Fig. 5A**). However, uptake of ^{131}I-IBA-CP was remarkably higher in MDA-MB-453 tumor than that in MCF-7 and MDA-MB-468 tumors (1.05 ± 0.25 *vs.* 0.32 ± 0.13 and 0.38 ± 0.05 %ID/g, $P < 0.001$) (**Fig. 5B**). Similarly, the tumor/muscle activity ratio was significantly higher in

the HER2-positive group than that of the two HER2-negative groups (6.0 ± 1.2 *vs.* 1.9 ± 0.7 and 1.3 ± 0.2, $P < 0.001$) (**Fig. 5C**).

The *in vivo* binding specificity and selectivity of ^{131}I-IBA-CP was further evaluated in two independent experiments. One group of mice (n = 4) bearing HER2-positive MDA-MB-453 tumor was sacrificed and examined at 3 h after the co-injection of an excess dose of nonradioactive IBA-CP with ^{131}I-IBA-CP. As expected, co-injection resulted in dramatically reduction in tumor uptake (from 1.05 ± 0.25 to 0.19 ± 0.04 %ID/g, $P < 0.001$), as well as in tumor/muscle activity ratio (from 6.0 ± 1.2 to 1.3 ± 0.1) (**Fig. 5**), while no significant changes in uptake were found in the blood or any other organs (**Fig. 5A**). In another independent group, we tested whether co-injection with erlotinib interfered with the binding of ^{131}I-IBA-CP. As seen in **Fig. 5**, the tumor uptake and tumor/muscle activity ratio were almost the same as those in the control group, indicating that erlotinib did not compete with the binding of the radiotracer. Hence, results from biodistribution studies further supported the *in vivo* binding specificity and selectivity of ^{131}I-IBA-CP toward HER2.

Biodistribution of ^{131}I-ICP at 3 h p.i. was also studied in mice bearing MDA-MB-453 tumors and compared with that of ^{131}I-IBA-CP. As shown in Supplemental Fig. 16, ^{131}I-ICP had much higher accumulation in the thyroid but less uptake in the tumor than ^{131}I-IBA-CP.

Molecular Modeling Studies

Docking of CP724,714 and IBA-CP to the HER2 receptor and EGFR (Supplemental Fig. 17) showed that IBA-CP provided more negative free energy of binding to HER2 than that to EGFR, at -10.28 kcal/mol and -8.74 kcal/mol, respectively. Significant differences were found by comparing the amino

acid residues and non-covalent bonding between docking of IBA-CP to HER2 and EGFR. For the HER2/IBA-CP system, there were three hydrogen bonds in the hinge region. There was also a halogen bond between the iodine atom of IBA-CP and the side chain of LYS753, and an aromatic hydrogen bond between the toluene fragment and the side chain of ASP863. However, there was no hinge region–interaction for the EGFR/IBA-CP complex. For comparison, CP724,714 displayed interactions with HER2 and EGFR similar to those of IBA-CP, with free energies of binding at -10.56 kcal/mol and -6.17 kcal/mol, respectively. Collectively, the structural modification of CP724,714 to IBA-CP did not influence its affinity and specificity towards the tyrosine kinase domain of HER2.

DISCUSSION

In this article, we demonstrated the feasibility of labeling the HER2 selective inhibitor CP724,714 and its analog, IBA-CP, as radiotracers. Two radioiodinated tracers, $^{125/131}$I-IBA-CP and $^{125/131}$I-ICP, were thus prepared for evaluation of their *in vitro* and *in vivo* binding characteristics and *in vivo* imaging properties. To the best of our knowledge, this is the first study to show that radiolabeled small molecule TKIs have the ability to image HER2 expression levels *in vivo*.

To reduce the radiosynthesis time, we labeled ^{125}I-IBA-CP or ^{131}I-IBA-CP by a copper-mediated radioiodination method using CuCl/1,10-phenanthroline as catalysts, which attached the radioiodine to an unactivated (nonphenolic) aromatic ring with high radiolabeling yield and molar activity (*36*). ^{125}I-IBA-CP exhibited excellent stability both *in vitro* and *in vivo*. *In vitro* biological activity assays indicated that, similar to CP724,714, IBA-CP was a HER2 selective tyrosine kinase inhibitor with negligible activity towards EGFR. As a small molecule HER2-selective TKI, ^{125}I-IBA-CP may have the ability to

penetrate the cell membrane and thus can be used to better identify the status of the intracellular HER2 kinase (*23*). The easy radiolabeling protocol and favorable stability of ^{125}I-IBA-CP, coupled with its good binding affinity and high selectivity for HER2, encouraged us to further investigate its potential for *in vivo* tumor imaging with SPECT.

SPECT/CT imaging and biodistribution studies with radioiodinated IBA-CP in mice revealed rapid and comparatively high uptake in the subcutaneous HER2-positive MDA-MB-453 tumor, and extremely low uptake in HER2-negative tumors (MDA-MB-468 and MCF-7). It is important to note that MDA-MB-468 cells have a high level of EGFR expression, hence the remarkably low uptake of ^{131}I-IBA-CP indicated the high selectivity of this radiotracer for HER2 over EGFR. The *in vivo* imaging results were well matched with findings from immunohistofluorescence and immunohistochemistry analyses. Additionally, uptake of ^{125}I-IBA-CP in HER2-positive tumors was effectively blocked by IBA-CP, but not by the EGFR inhibitor erlotinib, further demonstrating that the binding of ^{125}I-IBA-CP *in vivo* was receptor-mediated, specific, and selective for HER2.

In comparison, ^{125}I-ICP, prepared from direct radioiodination of CP724,714, displayed lower uptake in HER2 positive tumor than ^{125}I-IBA-CP, but higher accumulation in the liver region, which may be partly due to the higher lipophilicity of ^{125}I-ICP (log P value of 2.71 vs. 1.82 for ^{125}I-IBA-CP). Furthermore, it has been reported that CP724,714 could inhibit the hepatic efflux transporters, which contributed to its hepatic accumulation and bile constituents (*37*). The latter may be the main reason for the higher liver uptake of ^{125}I-ICP, which were also consistent with findings of high liver uptake in imaging studies with other TKIs (*38-40*).

CONCLUSION

Our results from the present study demonstrate that the radioiodinated IBA-CP is HER2 selective, and thus may be used to assess HER2 expression *in vivo* by SPECT/CT imaging. When validated in humans, applications of this novel imaging agent may include patient stratification via assessment of HER2 kinase expression levels, as well as dose optimization and therapeutic effect monitoring of HER2 kinase inhibitors through measurement of HER2 kinase inhibition and occupancy. Radionuclide-based imaging with a readily scalable synthetic small-molecule HER2 inhibitor is advantageous for clinical applications, due to its high affinity to the target receptor and fast clearance from the blood and normal organs. Nonetheless, the current imaging probe, although promising, displays only moderate specific binding signals. Further structure-activity optimization is needed to provide a radiotracer with improved *in vivo* performance, such as enhanced tumor uptake and reduced liver uptake.

ACKNOWLEDGMENTS

This study was financially supported by the National Key Basic Research Program of China (2014CB744503), National Natural Science Foundation of China (21271030, 81471707), and the Intramural Research Program, National Institute of Biomedical Imaging and Bioengineering, National Institutes of Health (ZIA EB000073).

REFERENCES

1. Yarden Y, Pines G. The ERBB network: at last, cancer therapy meets systems biology. *Nat Rev Cancer.* 2012;12:553-563.

2. Janjigian YY, Sanchez-Vega F, Jonsson P, et al. Genetic Predictors of Response to Systemic Therapy in Esophagogastric Cancer. *Cancer Discovery.* 2018;8:49.

3. Sauter G, Lee J, Bartlett JM, Slamon DJ, Press MF. Guidelines for human epidermal growth factor receptor 2 testing: biologic and methodologic considerations. *J Clin Oncol.* 2009;27:1323-1333.

4. Wolff AC, Hammond MEH, Hicks DG, et al. Recommendations for Human Epidermal Growth Factor Receptor 2 Testing in Breast Cancer: American Society of Clinical Oncology/College of American Pathologists Clinical Practice Guideline Update. *J Clin Oncol.* 2013;31:3997-4013.

5. Scartozzi M, Bearzi I, Berardi R, Mandolesi A, Fabris G, Cascinu S. Epidermal growth factor receptor (EGFR) status in primary colorectal tumors does not correlate with EGFR expression in related metastatic sites: implications for treatment with EGFR-targeted monoclonal antibodies. *J Clin Oncol.* 2004;22:4772-4778.

6. Zidan J, Dashkovsky I, Stayerman C, Basher W, Cozacov C, Hadary A. Comparison of HER-2 overexpression in primary breast cancer and metastatic sites and its effect on biological targeting therapy of metastatic disease. *Brit J Cancer.* 2005;93:552.

7. Capala J, Bouchelouche K. Molecular imaging of HER2-positive breast cancer: a step toward an individualized 'image and treat' strategy. *Curr Opin Oncol.* 2010;22:559-566.

8. Gebhart G, Flamen P, De Vries EGE, Jhaveri K, Wimana Z. Imaging Diagnostic and Therapeutic Targets: Human Epidermal Growth Factor Receptor 2. *J Nucl Med.* 2016;57:81S-88S.

9. Pereira PMR, Abma L, Henry KE, Lewis JS. Imaging of human epidermal growth factor receptors for patient selection and response monitoring - From PET imaging and beyond. *Cancer Lett.* 2018;419:139-151.

10. Henry KE, Ulaner GA, Lewis JS. Human Epidermal Growth Factor Receptor 2-Targeted PET/Single-Photon Emission Computed Tomography Imaging of Breast Cancer: Noninvasive Measurement of a Biomarker Integral to Tumor Treatment and Prognosis. *PET Clin.* 2017;12:269-288.

11. Ulaner GA, Hyman DM, Lyashchenko SK, Lewis JS, Carrasquillo JA. ^{89}Zr-Trastuzumab PET/CT for Detection of Human Epidermal Growth Factor Receptor 2–Positive Metastases in Patients With Human Epidermal Growth Factor Receptor 2–Negative Primary Breast Cancer. *Clin Nucl Med.* 2017;42:912-917.

12. Ulaner GA, Lyashchenko SK, Riedl C, et al. First-in-human HER2-targeted imaging using (89)Zr-pertuzumab PET/CT: Dosimetry and clinical application in patients with breast cancer. *J Nucl Med.* 2017.

13. Cai W, Niu G, Chen X. Multimodality imaging of the HER-kinase axis in cancer. *Eur J Nucl Med Mol Imaging.* 2008;35:186-208.

14. Corcoran EB, Hanson RN. Imaging EGFR and HER2 by PET and SPECT: a review. *Med Res Rev.* 2014;34:596.

15. Mortimer JE, Bading JR, Colcher DM, et al. Functional imaging of human epidermal growth factor receptor 2–positive metastatic breast cancer using ^{64}Cu-DOTA-trastuzumab PET. *J Nucl Med.* 2014;55:23-29.

16. Mendler CT, Gehring T, Wester H-J, Schwaiger M, Skerra A. ^{89}Zr-Labeled Versus ^{124}I-Labeled αHER2 Fab with Optimized Plasma Half-Life for High-Contrast Tumor Imaging In Vivo. *J Nucl Med.* 2015;56:1112-

1118.
17. Pruszynski M, Koumarianou E, Vaidyanathan G, et al. Improved tumor targeting of anti-HER2 nanobody through N-succinimidyl 4-guanidinomethyl-3-iodobenzoate radiolabeling. *J Nucl Med.* 2014;55:650-656.
18. Reddy S, Shaller CC, Doss M, et al. Evaluation of the anti-HER2 C6.5 diabody as a PET radiotracer to monitor HER2 status and predict response to trastuzumab treatment. *Clin Cancer Res.* 2011;17:1509-1520.
19. Baum RP, Prasad V, Muller D, et al. Molecular imaging of HER2-expressing malignant tumors in breast cancer patients using synthetic 111In- or 68Ga-labeled affibody molecules. *J Nucl Med.* 2010;51:892-897.
20. Niu G, Cai W, Chen X. Molecular imaging of human epidermal growth factor receptor 2 (HER-2) expression. *Front Biosci.* 2008;13:790-805.
21. Lee S, Xie J, Chen X. Peptides and peptide hormones for molecular imaging and disease diagnosis. *Chem Rev.* 2010;110:3087.
22. Li L, Wu Y, Wang Z, et al. SPECT/CT Imaging of the Novel HER2-targeted Peptide Probe ^{99m}Tc-HYNIC-H6F in Breast Cancer Mouse Models. *J Nucl Med.* 2017;58:821.
23. Gerstle J, Shahul S, Mahmood F. Radiolabelled receptor-tyrosine-kinase targeting drugs for patient stratification and monitoring of therapy response: prospects and pitfalls. *Lancet Oncology.* 2010;11:992-1000.
24. Goldstein R, Sosabowski J, Vigor K, Chester K, Meyer T. Developments in single photon emission computed tomography and PET-based HER2 molecular imaging for breast cancer. *Expert Rev Anticancer Ther.* 2013;13:359-373.
25. Memon AA, Jakobsen S, Dagnaes-Hansen F, Sorensen BS, Keiding S, Nexo E. Positron emission tomography (PET) imaging with ^{11}C-labeled erlotinib: a micro-PET study on mice with lung tumor xenografts. *Cancer Res.* 2009;69:873.
26. Gelovani JG. Molecular imaging of epidermal growth factor receptor expression-activity at the kinase level in tumors with positron emission tomography. *Cancer Metastasis Rev.* 2008;27:645-653.
27. Corcoran EB, Hanson RN. Imaging EGFR and HER2 by PET and SPECT: a review. *Med Res Rev.* 2014;34:596-643.
28. Gniazdowska E, Koźmiński P, Bańkowski K, W Ł, Królicki L. Synthesis, physicochemical and biological evaluation of technetium-99m labeled lapatinib as a novel potential tumor imaging agent of Her-2 positive breast cancer. *Eur J Med Chem.* 2014;87:493-499.
29. Nagasawa J, Mizokami A, Koshida K, Yoshida S, Naito K, Namiki M. Novel HER2 selective tyrosine kinase inhibitor, TAK-165, inhibits bladder, kidney and androgen-independent prostate cancer in vitro and in vivo. *Int J Urol.* 2006;13:587-592.
30. Zhou Y, Brattain MG. Synergy of epidermal growth factor receptor kinase inhibitor AG1478 and ErbB2 kinase inhibitor AG879 in human colon carcinoma cells is associated with induction of apoptosis. *Cancer Res.* 2005;65:5848-5856.
31. Barbacci EG, Pustilnik LR, Rossi AM, et al. The biological and biochemical effects of CP-654577, a selective erbB2 kinase inhibitor, on human breast cancer cells. *Cancer Res.* 2003;63:4450-4459.
32. Jani JP, Barbacci G, Bhattacharya S, et al. CP-724714, a novel erbB2 receptor tyrosine kinase inhibitor for cancer therapy. *Cancer Res.* 2004;64.
33. Jani JP, Finn RS, Campbell M, et al. Discovery and pharmacologic characterization of CP-724,714, a selective ErbB2 tyrosine kinase inhibitor. *Cancer Res.* 2007;67:9887.
34. Kath JC, Bhattacharya, Samit Kumar, Morris, Joel, Kath JC, Bhattacharya, Samit Kumar, Morris,

JoelKath JC, Bhattacharya, Samit Kumar, Morris, Joels; Pfizer Products Inc., USA., assignee. Preparation of substituted 4-quinazolinamines for the treatment of abnormal cell growth. US patent WO2001098277A2, 2001.

35. Zhang P, Zhuang R, Guo Z, Su X, Chen X, Zhang X. A Highly Efficient Copper-Mediated Radioiodination Approach Using Aryl Boronic Acids. *Chem-Eur J*. 2016;22:16783-16786.

36. Zhang P, Zhuang R, Wang X, et al. Highly Efficient and Stable Strain-Release Radioiodination for Thiol Chemoselective Bioconjugation. *Bioconjugate Chem.* 2018;29:467–472

37. Feng B, Xu JJ, Bi YA, et al. Role of hepatic transporters in the disposition and hepatotoxicity of a HER2 tyrosine kinase inhibitor CP-724,714. *Toxicol Sci.* 2009;108:492-500.

38. Doubrovin M, Kochetkova T, Santos E, et al. ^{124}I-iodopyridopyrimidinone for PET of Abl kinase-expressing tumors in vivo. *J Nucl Med.* 2010;51:121-129.

39. Song H, Li Y, Lee J, Schwartz AL, Bu G. Low-density lipoprotein receptor-related protein 1 promotes cancer cell migration and invasion by inducing the expression of matrix metalloproteinases 2 and 9. *Cancer Res.* 2009;69:879.

40. Su H, Seimbille Y, Ferl GZ, et al. Evaluation of [^{18}F]gefitinib as a molecular imaging probe for the assessment of the epidermal growth factor receptor status in malignant tumors. *Eur J Nucl Med Mol Imaging.* 2008;35:1089-1099.

Figures and Figure Legends

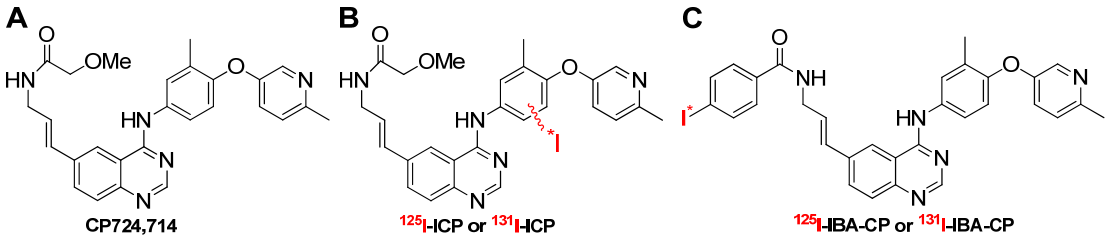

FIGURE 1. The chemical structures of CP724,714 (A), ^{125}I or ^{131}I-labeled CP724,714 (B) and its analog (C).

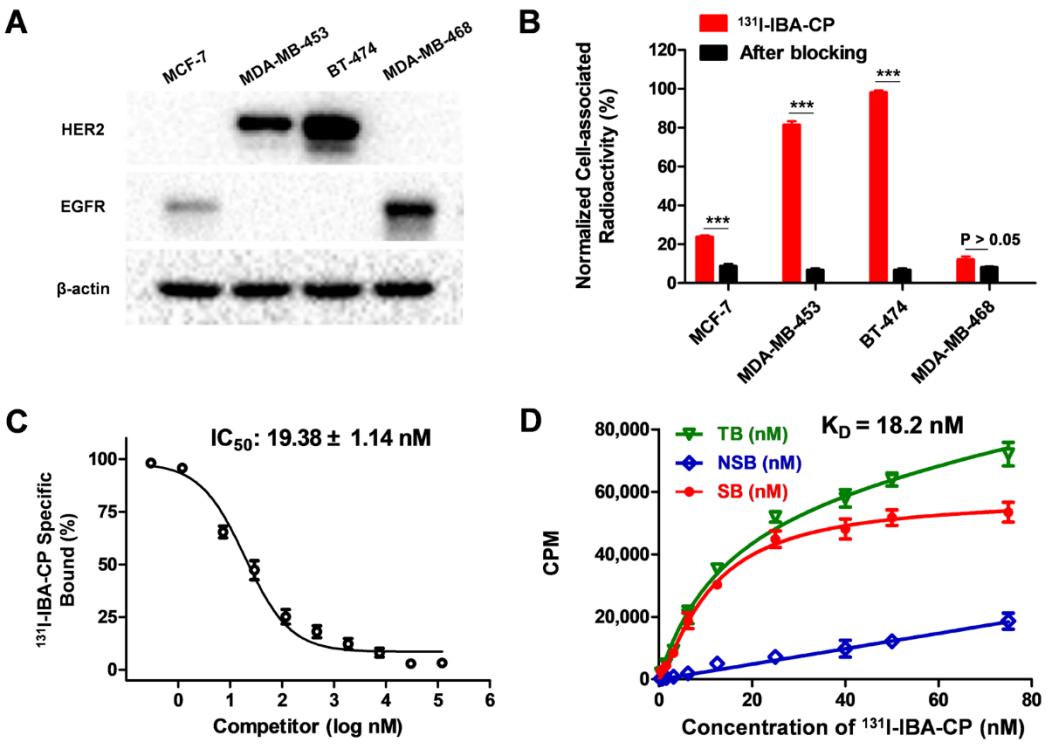

FIGURE 2. (A) HER2 and EGFR protein levels in different cells evaluated by WB. (B) The binding of ^{131}I-IBA-CP to cells with different levels of HER2 expression (cell line versus normalized cell-associated radioactivity (%) and the effect of preincubation with IBA-CP on the binding. The data are shown as mean ± SD (n = 3), *** indicated $P < 0.001$). (C) Representative results of competition-binding assay using MDA-MB-453 cells. (D) Representative results of saturation assay using MDA-MB-453 cells.

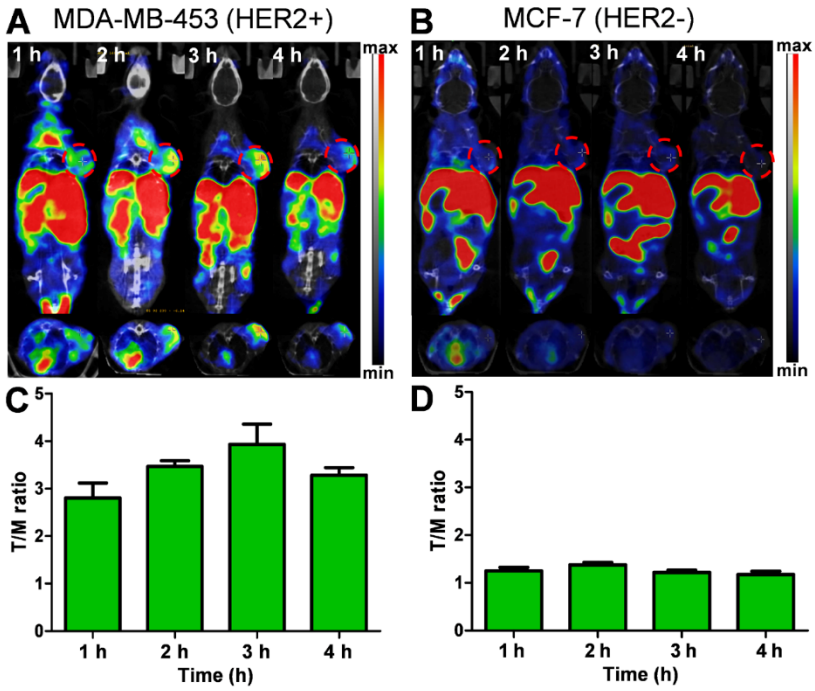

FIGURE 3. (A-B) Representative SPECT/CT images obtained at 1, 2, 3 and 4 h after injection of ^{125}I-IBA-CP in MDA-MB-453 (A) and MCF-7 (B) tumor-bearing mice. (C-D) Tumor-to-muscle ratios obtained from A (C) and B (D). (n = 3, error bars correspond to standard deviation; Circles indicate tumors)

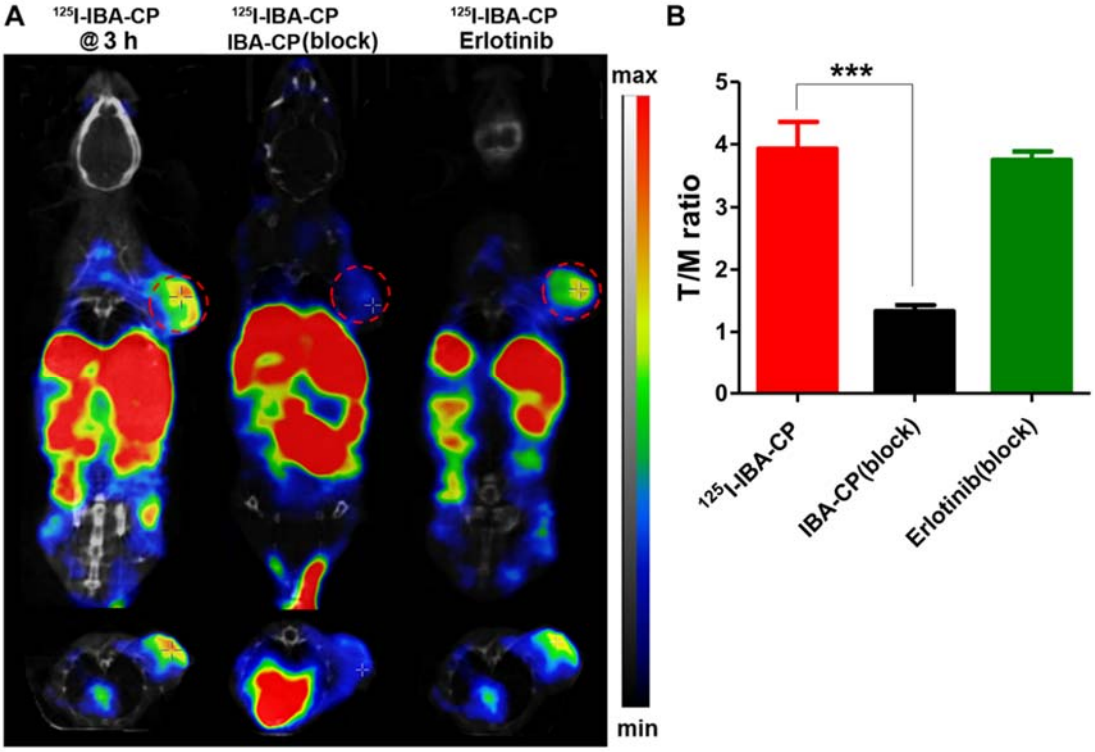

FIGURE 4. (A) Representative SPECT/CT images obtained at 3 h after injection of ^{125}I-IBA-CP in MDA-MB-453 tumor-bearing mice with or without blocking doses of nonradioactive compound IBA-CP or erlotinib. (B) Quantification of the SPECT imaging results. (Circles indicate tumors; n = 3, ***P < 0.001; Data are means ± SD)

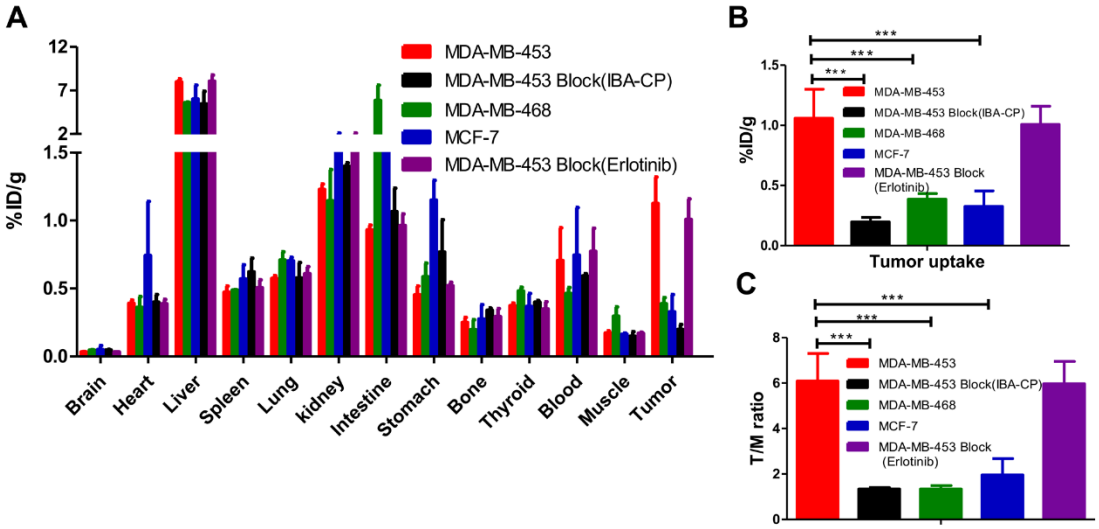

FIGURE 5. (A) Biodistribution of ^{131}I-IBA-CP in MDA-MB-453 (HER2+), MDA-MB-468 (HER2-, EGFR+) and MCF-7 (HER2-) tumor-bearing nude mice at 3 h after injection and in MDA-MB-453 tumor-bearing nude mice co-injected with nonradioactive compound IBA-CP or Erlotinib as blocking agent at 30 min after injection. (B), (C) ^{131}I-IBA-CP tumor uptake values and tumor/muscle ratio from A. (n = 4, ***P < 0.001; Data are means ± SD)

SUPPLEMENTAL INFORMATION FILE

Radioiodinated Small Molecule Tyrosine Kinase Inhibitor as a Novel Tracer for HER2 Selective Targeting

Longguang Tang[1,2#], Chenyu Peng[1#], Bowen Tang[3], Zijing Li[1]*, Xiangyu Wang[1], Jindian Li[1], Fei Gao[1], Lumei Huang[1], Duo Xu[1], Pu Zhang[1], Rongqiang Zhuang[1], Xinhui Su[4], Xiaoyuan Chen[2] and Xianzhong Zhang[1]*

[1]State Key Laboratory of Molecular Vaccinology and Molecular Diagnostics & Center for Molecular Imaging and Translational Medicine, School of Public Health, Xiamen University, Xiamen 361005, China

[2]Laboratory of Molecular Imaging and Nanomedicine (LOMIN), National Institute of Biomedical Imaging and Bioengineering (NIBIB), National Institutes of Health, Bethesda, Maryland 20892, United States

[3]School of Pharmaceutical Science, Xiamen University, Xiamen 361005, China

[4]Zhongshan Hospital Affiliated of Xiamen University, Xiamen 361004, China.

SUPPLEMENTAL MATERIAL & METHODS

Cell Culture and Animal Models

Human breast cancer cell lines (BT-474, MDA-MB-453, MCF-7, and MDA-MB-468) were obtained from China Infrastructure of Cell Line Resources. The cells were cultured in RPMI 1640 medium (BT-474, MCF-7 and MDA-MB-468) or in Leibovitz L15 medium (MDA-MB-453) supplemented with 10% (v/v) heat-inactivated fetal bovine serum (GIBCO) and penicillin/streptomycin (concentration of 100 U/mL for each). Cells were grown as a monolayer at 37 °C in a humidified atmosphere containing 5% CO_2.

All animal studies were conducted in accordance with the guidelines of the Xiamen University Animal Care and Use Committee. Five- to 7-week-old female Balb/C nude mice were injected subcutaneously into the right front flanks with MDA-MB-453, MCF-7 or MDA-MB-468 cells (1×10^7 in 200 μL of phosphate-buffered saline). The animals were used for *in vivo* studies when the tumor size reached 100–150 mm^3 (2–3 wk after inoculation)

In Vitro Cell-binding Assays

The *in vitro* binding characteristics of ^{131}I-IBA-CP were assessed using saturation and displacement cell-binding assays. The specificity of binding was also tested for cell lines with different levels of HER2 expression. For binding assays, ^{131}I-IBA-CP was prepared in high specific activity (42 MBq/nmol) and the unlabeled IBA-CP was used as the competitor. Experiments were performed in triplicates according to the previously reported method (*1*). In brief, the day before the experiments, cells were seeded in six-well plates at a concentration of 2.5×10^5 cells/mL. The cells were incubated (4 °C, 2 h) with 43 nM of ^{131}I-IBA-CP and increasing concentrations (0.30 nM - 120 μM) of unlabeled IBA-CP.

Measurement of Lipophilicity (log P)

The radiolabeled compound (^{125}I-IBA-CP or ^{125}I-ICP, 0.74 MBq each) was mixed with equal volume of n-octanol (0.9 mL) and PBS buffer (pH 7.4, 1 mL), vortexed for 2 min, and then centrifuged at 10000 rpm for 2 min at room temperature to partition the layers. Aliquots of 0.1 mL each were taken from the organic and aqueous layers and counted in a well-type γ-counter. Distribution coefficient P was calculated as the ratio of activity in the organic to that in the aqueous phase (as an average value from at least three independent measurements). The partition was done for three times and the log P values were taken from the third partition.

SUPPLEMENTAL TABLES

Supplemental Table 1. Lipophilicity (log P) of ^{125}I-IBA-CP and ^{125}I-ICP.

Compounds	log P
^{125}I-IBA-CP	1.82±0.24
^{125}I-ICP	2.71±0.21

Supplemental Table 2. In vitro enzymatic activities of 9 (IBA-CP) and CP724,714 against HER2.

Compounds	IC_{50} (nM, mean ± SD)*
9 (IBA-CP)	16.5± 2.1
CP724,714	11.3 ± 1.5

*** *In Vitro* Inhibition of HER2 Kinase**: The HER2 kinases reactions were performed and IC_{50} values calculated as previously described (*2*).

Supplemental Table 3. *In vitro* activity profile of 9 (IBA-CP) and CP724,714 against a panel of six cancer-related kinases.

Kinase	IBA-CP IC_{50} (nM, mean ± SD)	CP724,714 IC_{50} (nM, mean ± SD)
EGFR	2,340.3 ± 12.5	2,200.5± 5.6
HER4	>10,000	260
FGFR-1	>10,000	>10,000
PDGFRβ	>10,000	>10,000
VEGFR-2	>10,000	>10,000
c-Met	>10,000	>10,000

***In Vitro* Inhibition of Kinases and Selectivity Assays:** Reactions for the six kinases were performed and IC_{50} values calculated as previously descried (*2*).

SUPPLEMENTAL FIGURES

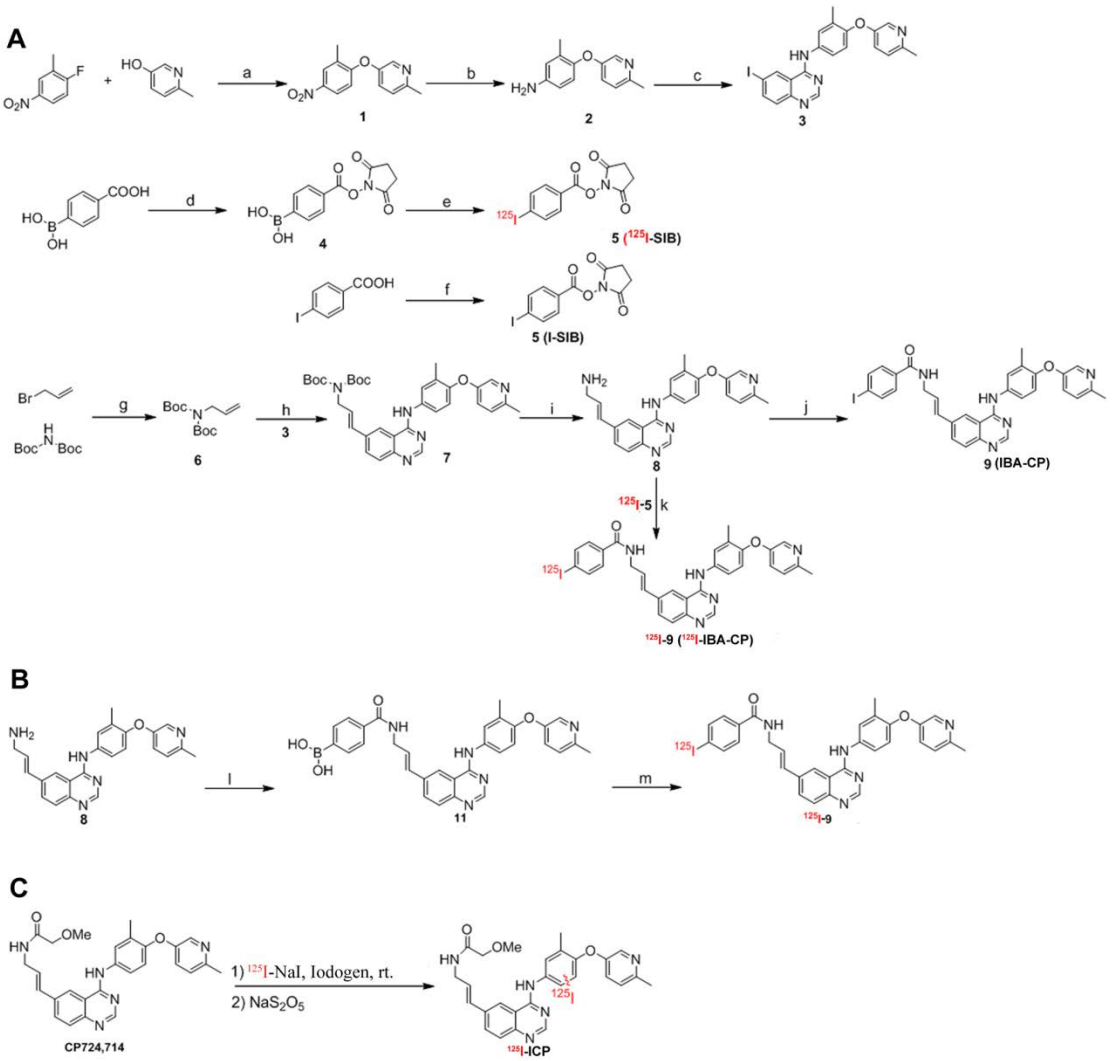

Supplemental Fig. 1. Synthesis routes of unlabeled IBA-CP, and radio-labeled ^{125}I-IBA-CP and ^{125}I-ICP. (A) Synthesis of IBA-CP and ^{125}I-IBA-CP by a two-step radiolabeling procedure. Reagents and conditions: a) K_2CO_3, DMF, 110 °C; b) 10 % Pd/C, H_2, MeOH; c) 4-chloro-6-iodoquinazoline, ^{i}-PrOH, reflux for 2 h, 25 °C for 6 h; d) NHS, EDCI, DIPEA, THF, rt.; e) Cu_2O, 1,10-phenanthroline, ^{125}I-NaI, CH_3CN (anhydrous), 1 h, 25 °C; f) NHS, EDCI, DIPEA, THF, rt.; g) K_2CO_3, CH_3CN, rt.; h) $Pd_2(dba)_3$, ^{i}-PrOH, Et_3N, N_2, 78 °C; i) concentrated HCl, rt.; j) 4-iodobenzoic acid, EDCI, HOBt, DIPEA, rt.; k) DIPEA, DMF, rt.. (B) Synthesis of ^{125}I-IBA-CP by a one-step radiolabeling procedure. Reagents and conditions: l) 4-boronobenzoic acid, EDCI, HOBt, DIPEA, rt.; m) CuCl, 1,10-phenanthroline, ^{125}I-NaI, CH_3CN, 1 h, rt. (C) Direct radioiodination of CP274,714 to produce ^{125}I-ICP.

Method: For the two-step synthesis of ^{125}I-IBA-CP, the intermediate ^{125}I-SIB was first prepared as previously described (*3*). Then, compound 8 (1.0 mg) was dissolved in 50 μL anhydrous DMF and

a triethylamine (5 μL) added. ^{125}I-SIB in anhydrous acetonitrile (40-70 MBq) was added to the solution and reacted for 1 h. The mixture was filtered and injected onto the semipreparative radio-HPLC column (Luna C-18, 5 μm, 10×250 mm; Thermo). The mobile phase was acetonitrile/water/trifluoroacetic acid (50:50:0.001 v/v), with a flow rate of 3 mL/min. The product was dissolved in phosphate buffer (0.05 M, pH 7.4) with expected activity concentration and passed through 0.22-μm Millipore filter to afford a solution ready for i.v. injection. The total radiosynthesis time of ^{125}I-IBA-CP by the two-step method, including HPLC purification, was 150-180 min.

For the one-step synthesis of ^{125}I-IBA-CP, (E)-(4-((3-(4-((3-methyl-4-((6-methylpyridin-3-yl)oxy)phenyl)amino)quinazolin-6-yl)allyl)carbamoyl)phenyl)boronic acid (**11**, 2 μmol) was added into the reaction vial, followed by 100 μL of CuCl/1,10-phenanthroline solution in acetonitrile containing 0.4 μmol of CuCl and 0.8 μmol of 1,10-phenanthroline. Finally, ^{125}I-NaI (18.5-20 MBq) solution in 5 μL water was added to the mixture and reacted for 60 min at 25 °C. The mixture was filtered and loaded onto the semi-preparative radio-HPLC column (Luna C-18, 5 μm, 10×250 mm; Thermo) eluting with the mobile phase (A: 0.1% TFA in water; B: 0.1% TFA in CH3CN) at a flow rate of 3 mL/min according to the following The gradient program: 0-5 min, 0% of B; 5-10 min, 0%-50% of B; 10-15 min, 50% of B; 15-20 min, 50%-0% of B. The total radiosynthesis time of ^{125}I-IBA-CP or ^{131}I-IBA-CP by the one-step method was 80-100 min.

^{125}I-ICP was synthesized using the Iodogen method as previously reported (Cancer Res. 1990; 50: 783s). The product was purified by using the same HPLC method for ^{125}I-IBA-CP.

Eluent from HPLC was monitored by a radiation detector. The fraction containing the radioactive product was collected and the solvents evaporated by passing a stream of N_2 gas through the reaction vial. The residue was constituted in phosphate buffer (0.05 M, pH 7.4) with expected activity concentration. Finally, the solution was passed through 0.22-μm Millipore filter to afford a solution ready for i.v. injection.

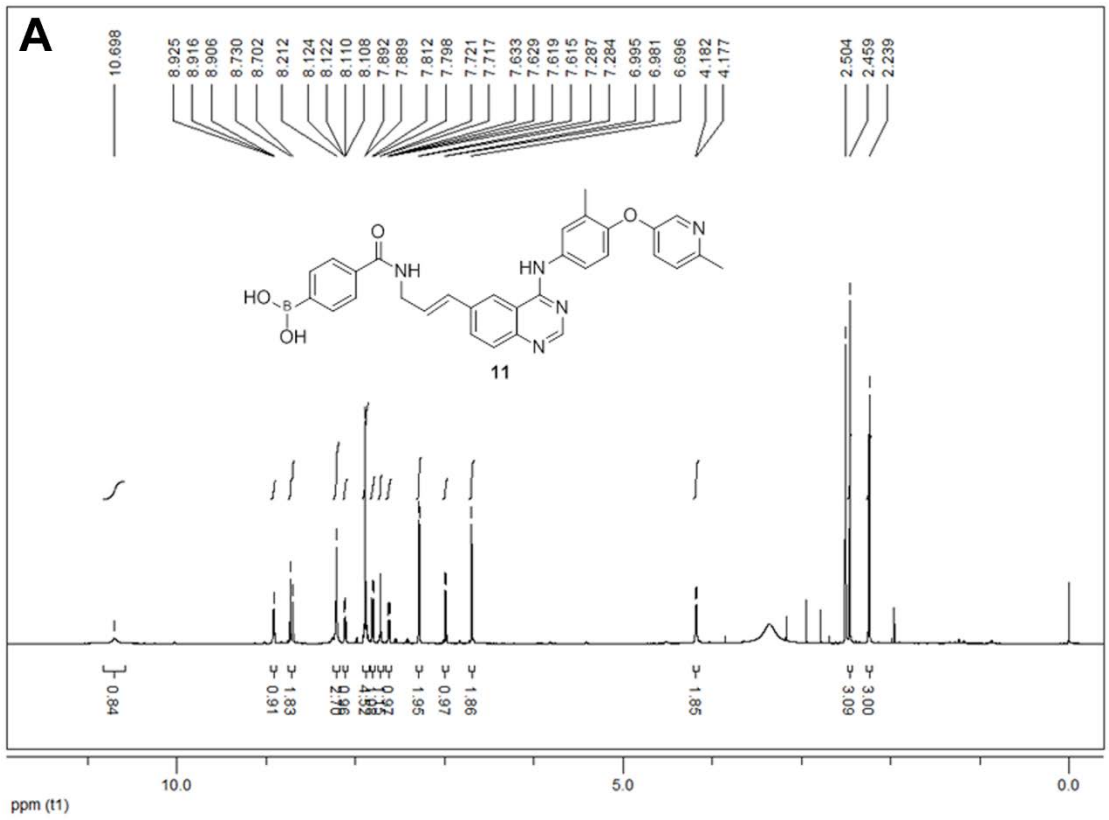
A
10.698
8.925
8.916
8.906
8.730
8.702
8.212
8.124
8.122
8.110
8.108
7.892
7.889
7.812
7.798
7.721
7.717
7.633
7.629
7.619
7.615
7.287
7.284
6.995
6.981
6.696
4.182
4.177
2.504
2.459
2.239
HO
B
OH
O
NH
HN
N
N
O
N
11
0.84
1.83
0.91
2.96
2.70
0.97
1.95
0.97
1.86
1.85
3.00
3.09
10.0
5.0
0.0
ppm (t1)

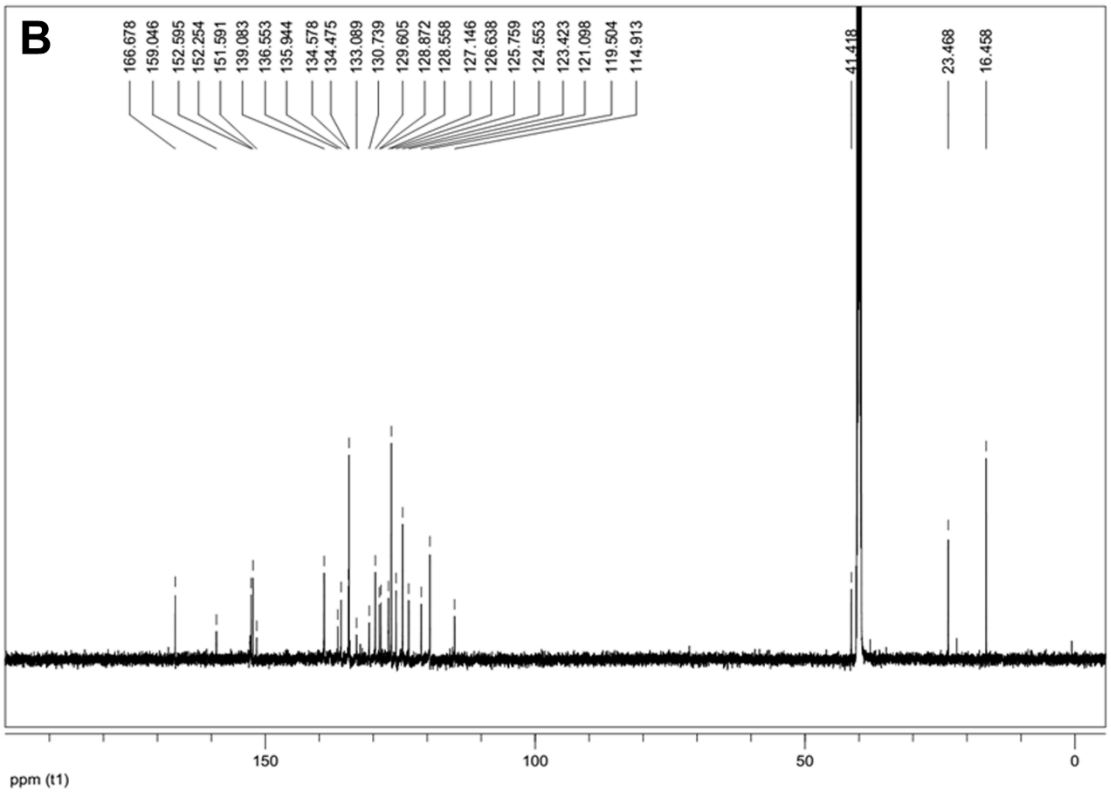
B
166.678
159.046
152.595
152.254
151.591
139.083
136.553
135.944
134.578
134.475
133.089
130.739
129.605
128.872
128.558
127.146
126.638
125.759
124.553
123.423
121.098
119.504
114.913
41.418
23.468
16.458
150
100
50
0
ppm (t1)

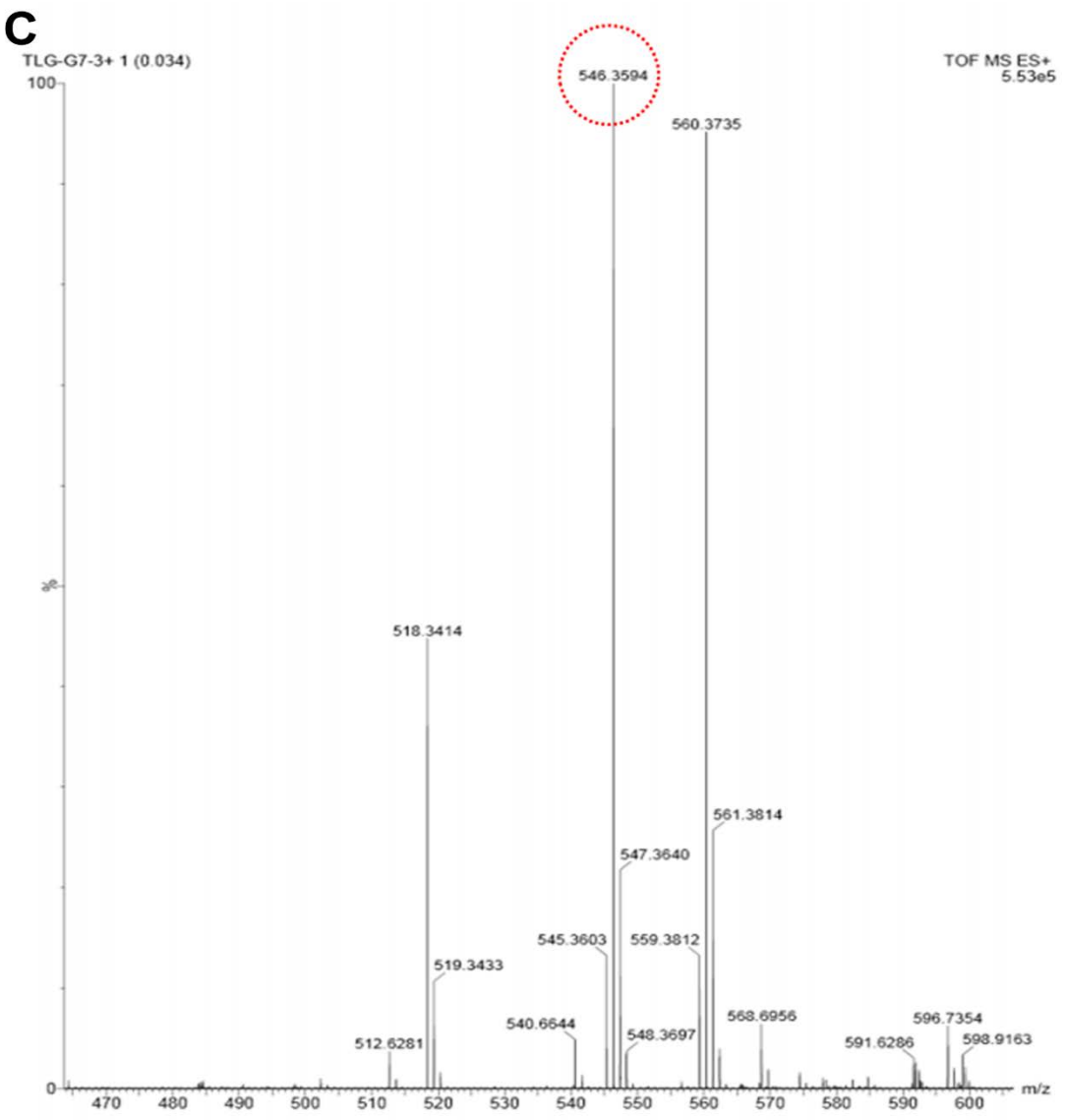

Supplemental Fig. 2. Precursor structural determination. Identification was performed by ^{1}H-NMR spectrum (A), ^{13}C-NMR spectrum (B) and mass spectrometry (C). (*E*)-(4-((3-(4-((3-Methyl-4-((6-methylpyridin-3-yl)oxy)phenyl)amino)quinazolin-6-yl)allyl)carbamoyl)phenyl)boronic acid (**11**). (A) ^{1}H-NMR (600 MHz, DMSO-d_6): δ (ppm) 10.689 (s, 1H), 8.916 (t, *J* = 5.4 Hz, 1H), 8.714 (d, *J* = 16.8 Hz, 2H), 8.212 (s, 3H), 8.117 (dd, *J* = 8.4 Hz, 1H), 7.892 (s, 4H), 7.805 (d, *J* = 8.4 Hz, 1H), 7.719 (s, 1H), 7.626 (dd, *J* = 8.4 Hz, 1H), 7.285 (s, 2H), 6.988 (d, *J* = 8.4 Hz, 1H), 6.696 (s, 2H), 4.179 (s, 2H), 2.459 (s, 3H), 2.239 (s, 3H); (B) **^{13}**C-NMR (150 MHz, DMSO-d_6): δ (ppm) = 166.678, 159.046, 152.595,152.254, 151.591, 139.083, 136.553, 135.944, 134.578, 134.475, 133.089, 130.739, 129.605, 128.872, 128.558, 127.146, 126.638, 125.759, 124.553, 123.423, 121.098, 119.504, 114.913, 41.418, 23.468, 16.458; (C) HRMS/EI: calcd for $C_{31}H_{28}BN_5O_4$ $[M + H]^+$ 546.2234; found 546.3594.

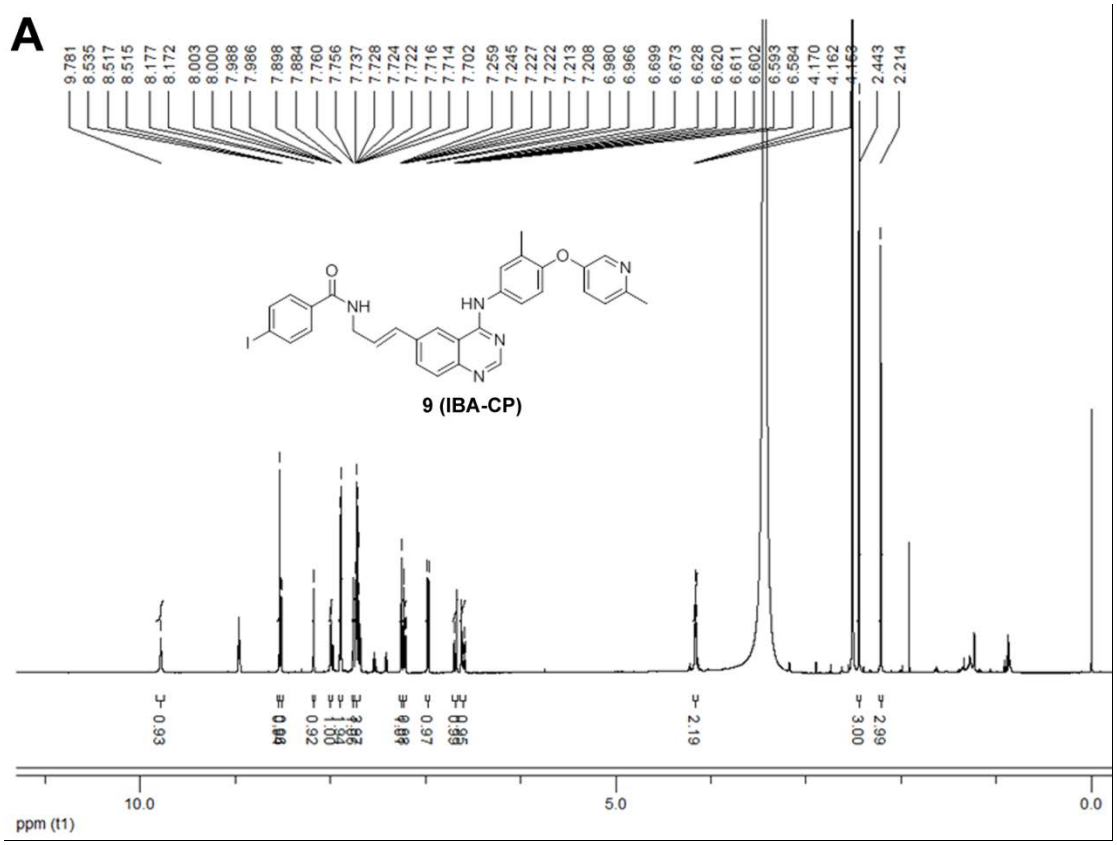
A
9.781
8.535
8.517
8.515
8.177
8.172
8.003
8.000
7.988
7.986
7.898
7.884
7.760
7.756
7.737
7.728
7.724
7.722
7.716
7.714
7.702
7.259
7.245
7.227
7.222
7.213
7.208
6.980
6.966
6.699
6.673
6.628
6.620
6.611
6.602
6.593
6.584
4.170
4.162
4.153
2.443
2.214
O
NH
HN
N
I
9 (IBA-CP)
0.93
0.92
0.97
2.19
3.00
2.99
10.0
5.0
0.0
ppm (t1)

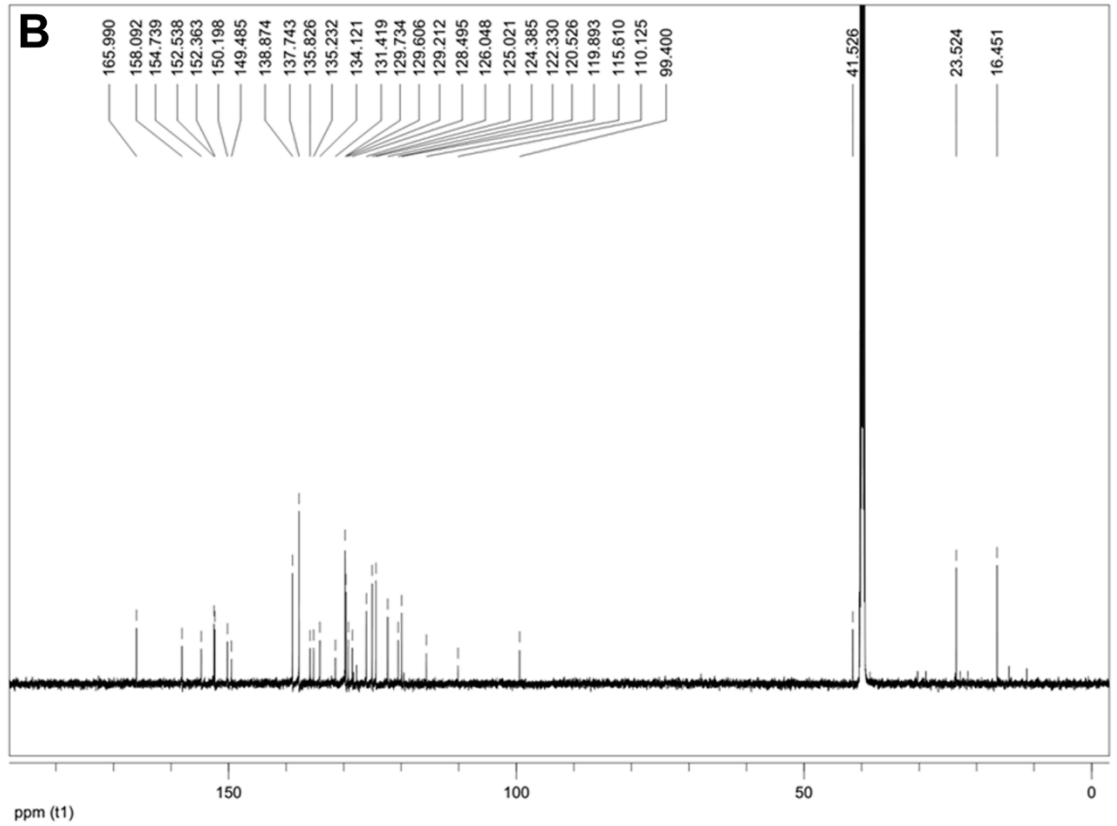
B
165.990
158.092
154.739
152.538
152.363
150.198
149.485
138.874
137.743
135.826
135.232
134.121
131.419
129.734
129.606
129.212
128.495
126.048
125.021
124.385
122.330
120.526
119.893
115.610
110.125
99.400
41.526
23.524
16.451
150
100
50
0
ppm (t1)

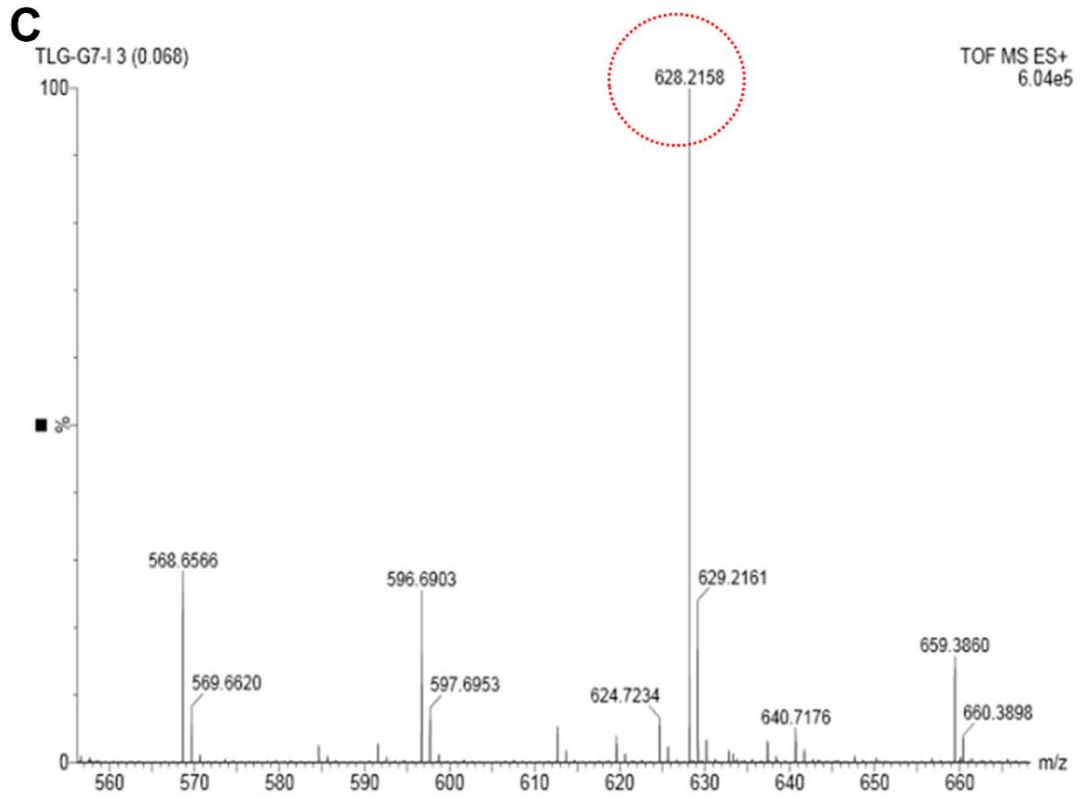

Supplemental Fig. 3. Confirmation of IBA-CP identity by ^{1}H-NMR, ^{13}C-NMR (B) and mass spectrometry (C). (*E*)-4-iodo-N-(3-(4-((3-methyl-4-((6-methylpyridin-3-yl)oxy)phenyl)amino)quinazolin-6-yl)allyl)benzamide (**9**, IBA-CP). (A) ^{1}H-NMR (600 MHz, DMSO-d_6): δ (ppm) 9.781 (s, 1H), 8.957 (t, *J* = 6 Hz, 1H), 8.535 (s, 1H), 8.516 (s, 1H), 8.174 (d, *J* = 3 Hz, 1H), 7.995 (dd, *J* =9Hz, *J* = 1.8 Hz, 1H), 7.891 (d, *J* = 8.4 Hz, 2H), 7.758 (s, 1H), 7.684-7.737 (m, 4H), 7.252 (d, *J* = 8.4 Hz, 1H), 7.208-7.227 (q, 1H), 6.973 (d, *J* = 8.4 Hz, 1H), 6.686 (d, *J* = 15.6 Hz, 1H), 6.584-6.628 (m, 1H), 4.162 (t, *J* = 4.8 Hz, 2H), 2.443 (s, 3H), 2.214 (s, 3H); (B) **^{13}**C-NMR (150 MHz, DMSO-d_6): δ (ppm) 165.990, 158.092, 154.739, 152.538, 152.363, 150.198, 149.485, 138.874, 137.743, 135.826, 135.232, 134.121, 131.419, 129.734, 129.606, 129.212, 128.495, 128.495, 126.048, 125.021, 124.385, 122.330, 120.526, 119.893, 115.610, 110.125, 99.400, 41.526, 23.524, 16.451; (C) HRMS/EI: calcd for $C_{31}H_{26}IN_5O_2$ $[M + H]^+$628.1131; found 628.2158.

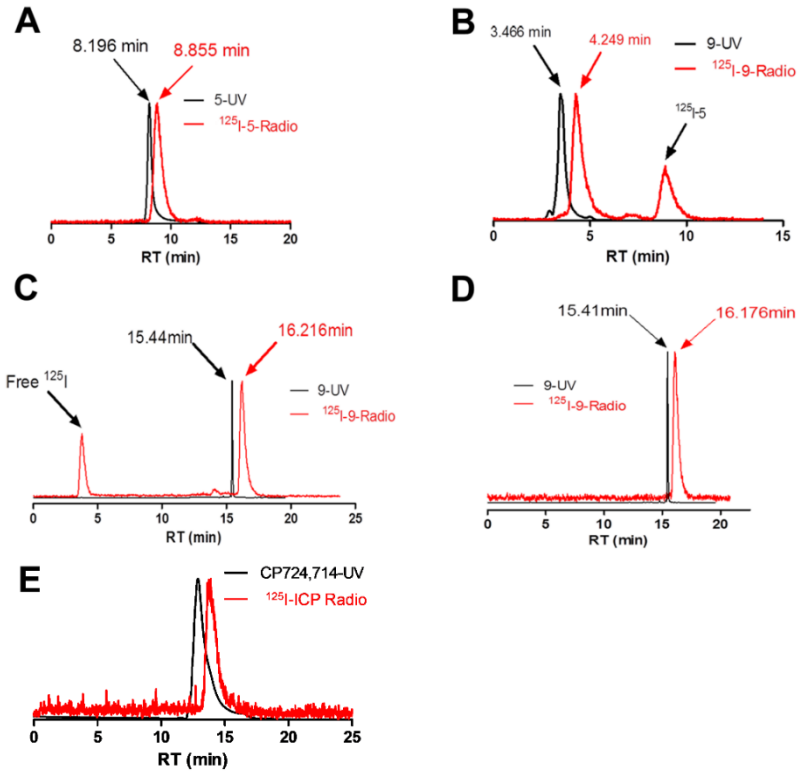

Supplemental Fig. 4. Analytical HPLC chromatograms of the crude reaction product from the preparation of ^{125}I-5 (A), and from two-step radiolabeling of ^{125}I-IBA-CP (B); HPLC chromatograms of the crude product from one-step radiolabeling of ^{125}I-IBA-CP (C) and purified ^{125}I-IBA-CP (D). Compound **5** or nonradioactive compound IBA-CP was injected separately as a reference standard to confirm the identity of the radiotracer. (E) Analytical HPLC chromatogram of purified ^{125}I-ICP and CP724,714, which serve as the non-radioactive reference standard.

At first, radio-intermediate ^{125}I-**5** was obtained in a radiochemical yield of 95.2 ± 3.4% (n = 6; based on HPLC analysis of the crude product) with a retention time of 8.86 min using analytical radio-HPLC. The mobile phase was acetonitrile/water/trifluoroacetic acid (50:50:0.001 v/v), and flow rate was 1 mL/min. ^{125}I-IBA-CP was then obtained through an amide coupling reaction between **8** and ^{125}I-**5** in 40 min, with a radiochemical yield of 67.1 ± 5.2% (n = 6; based on HPLC analysis of the crude product). The retention time of ^{125}I-IBA-CP was 4.25 min, which matched well with the corresponding nonradioactive compound IBA-CP (3.47 min) (the difference in retention times was mainly due to the dead volume (0.7~0.8 mL) between the UV and radioactivity detectors).

The precursor **11** was radiolabeled using CuCl/1,10-phenanthroline instead of Cu_2O/1,10-phenanthroline as a catalyst, with a radiochemical yield of 65.3 ± 5.2% (n = 6; as measured by HPLC). The gradient program of the mobile phase was as follows: 0-5 min, 0% of B (A: 0.1% TFA in water; B: 0.1% TFA in CH_3CN); 5-10 min, 0%-50% of B; 10-15 min, 50% of B; 15-20 min, 50%-0% of B.

After purification, the radiochemical purity of ^{125}I-IBA-CP was greater than 98% as determined by HPLC.

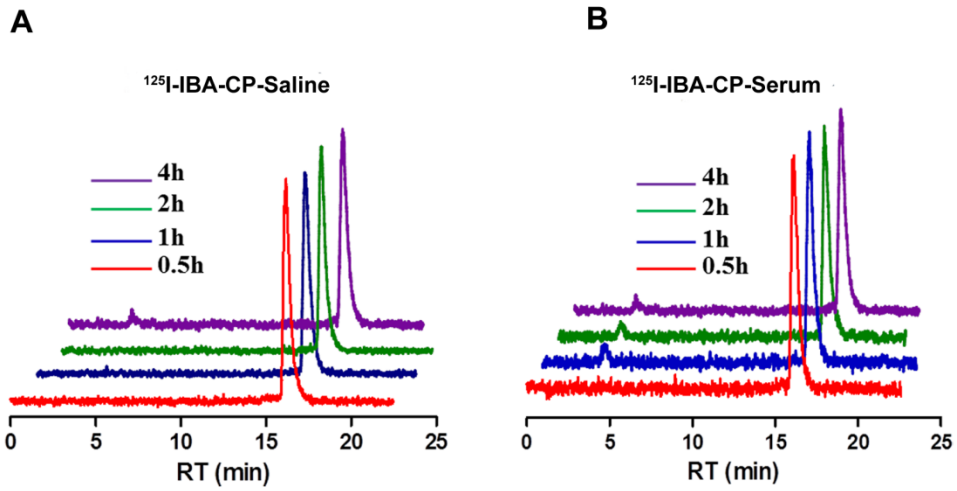

Supplemental Fig. 5. Determination of in vitro stability of ^{125}I-IBA-CP in saline (A) and mouse serum (B) by HPLC analysis. An aliquot of the ^{125}I-IBA-CP (370 kBq, 10 μCi) solution was added to 100 uL of normal saline, and then mixed with 500 μL of normal saline at 37 °C. Approximately 50 μL of the solution was then taken out and analyzed by radio-HPLC at 0.5 h, 1 h, 2 h and 4 h, respectively. Conditions for analytical HPLC were described as above. For *in vitro* stability testing of ^{125}I-IBA-CP in mouse plasma, a solution of the radiotracer (10 μCi) in 100 μL of normal saline was incubated with 500 μL of murine plasma at 37 °C for 0.5 h, 1 h, 2 h and 4 h, respectively. 100 μL of each above solution was precipitated by adding 200 μL of acetonitrile after centrifugating the plasma proteins at 5,000 rpm for 5 min at 4 °C. About 50 μL of the supernatant solution was loaded onto HPLC.

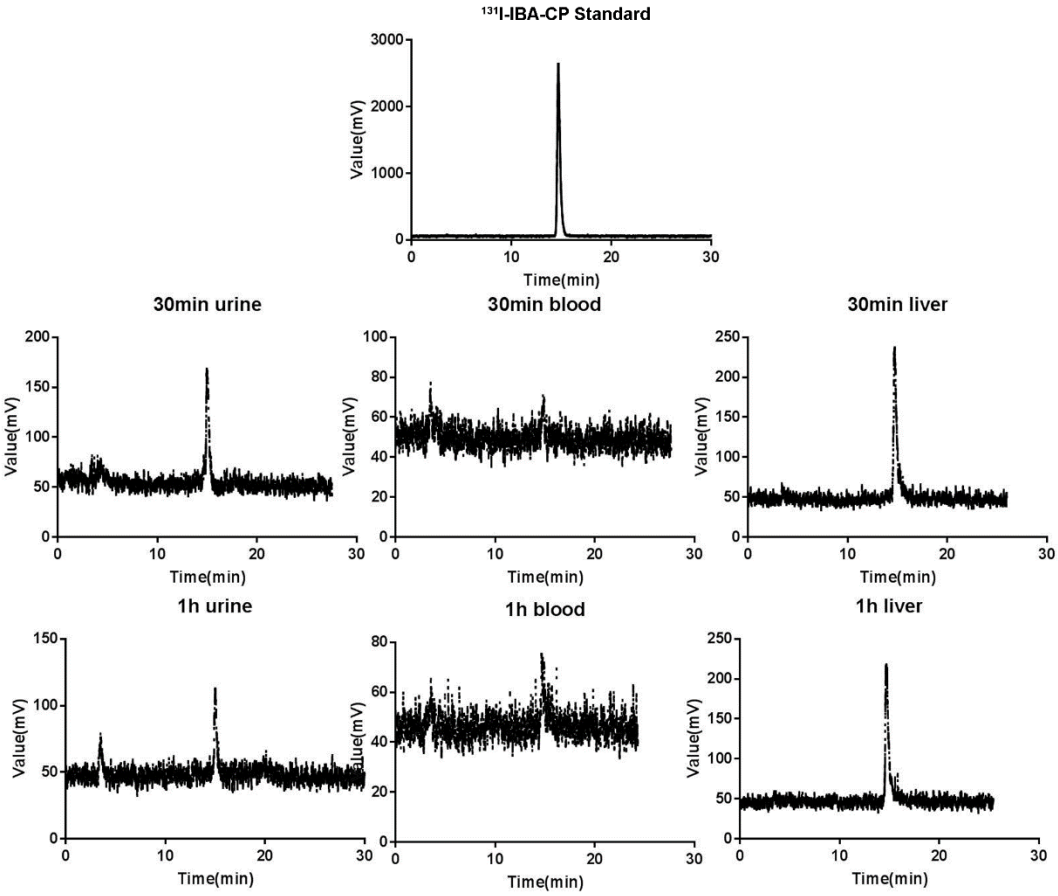

Supplemental Fig. 6. The *in vivo* metabolic stability of ^{131}I-IBA-CP. The *in vivo* metabolic stability of ^{131}I-IBA-CP was performed by detecting the radioactive metabolites in urine, blood, and liver at 30 min and 1 h post-injection time. The procedures were taken following the published reference (*4*) and the HPLC conditions were the same with the *in vitro* stability study.

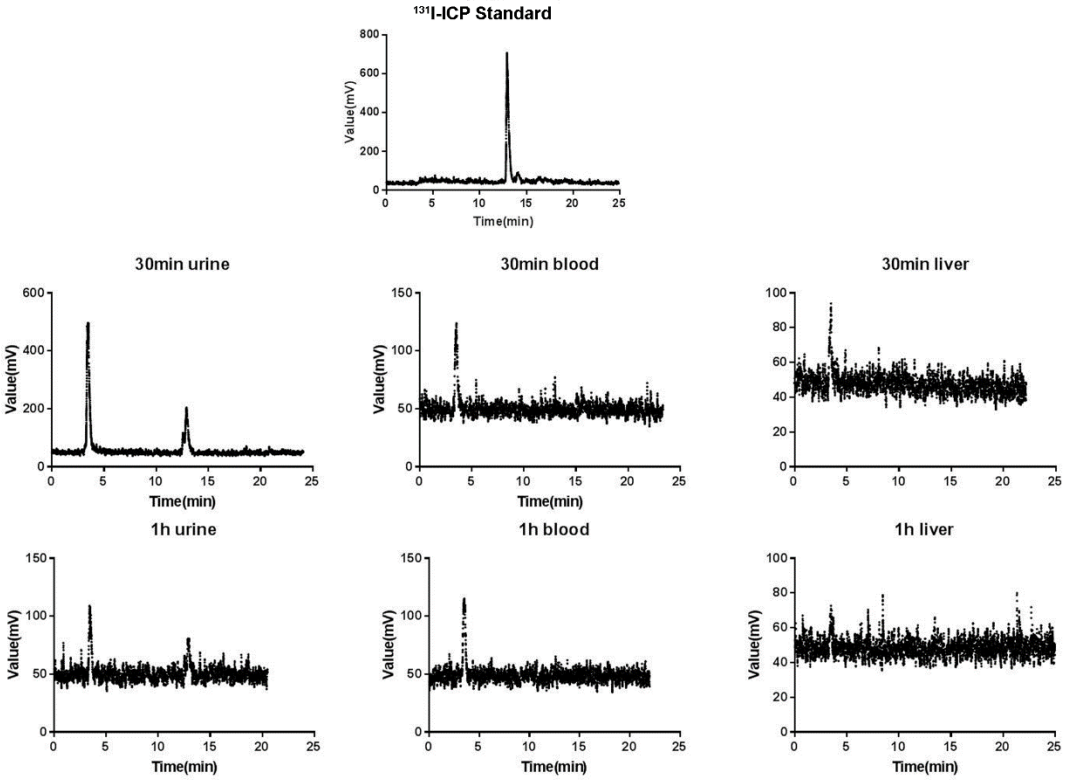

Supplemental Fig. 7. The *in vivo* metabolic stability of ^{131}I-ICP. The *in vivo* metabolic stability of ^{131}I-ICP was performed by detecting the radioactive metabolites in urine, blood, and liver at 30 min and 1 h post-injection time. The procedures were the same with that described in the *in vivo* metabolic stability study of ^{131}I-IBA-CP.

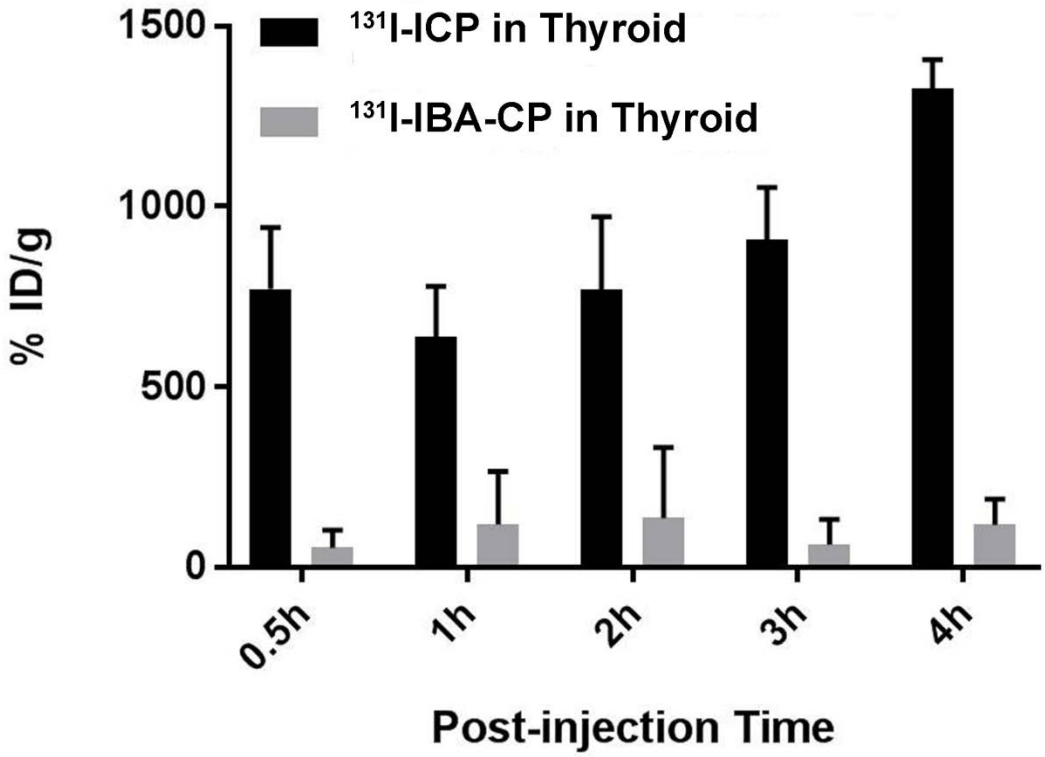

Supplemental Fig. 8. The uptake of ^{131}I-IBA-CP and ^{131}I-ICP in thyroids of normal mice.

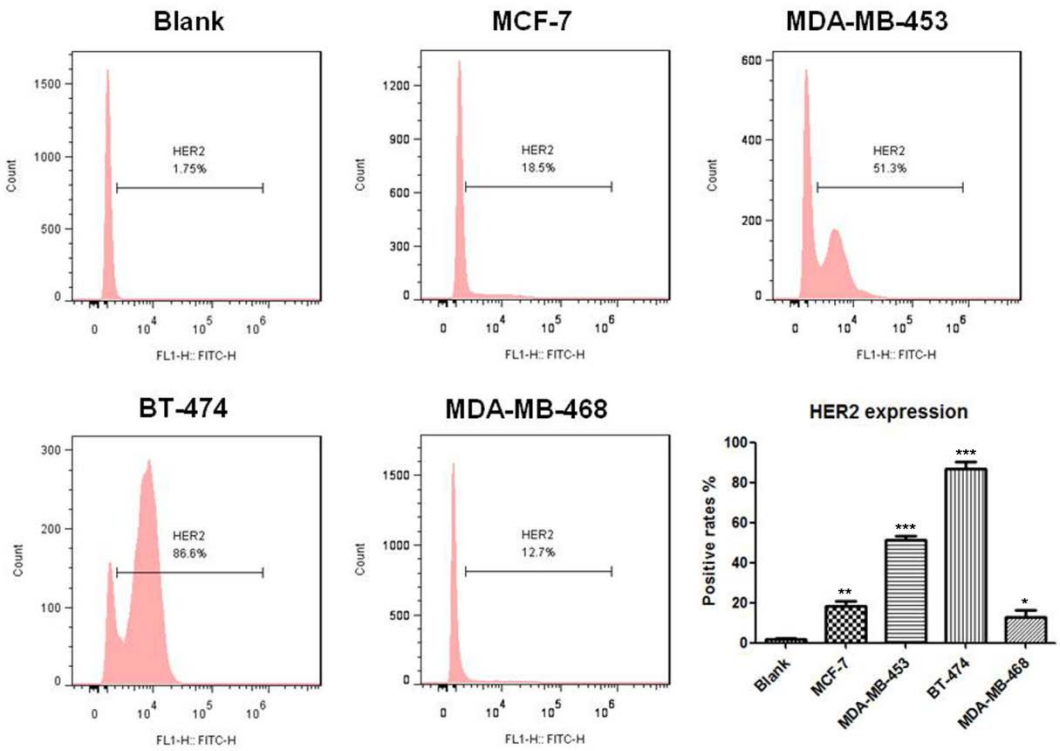

Supplemental Fig. 9. HER2 expression in different breast cancer cell lines measured by flow cytometry. (Compared with Blank group, *** $P < 0.001$)

Method: Human breast cancer cells (MCF-7, MDA-MB-453, BT-474, MDA-MB-468, 1×10^5 cells/mL) were collected, washed once with cold PBS, fixed with 4% paraformaldehyde (10 min) and then permeabilized with 0.1% PBS-Tween for 20 min. The cells were then incubated in 1x PBS/10% normal goat serum/0.3 M glycine to block non-specific protein-protein interactions followed by incubation with the antibody (ab134182, ab52894, Abcam) at 4°C overnight. The secondary antibody Goat Anti-Rabbit IgG H&L (FITC) (ab97050, Abcam) was used with 1/100 dilution and incubated for 30 min at 22 °C. Stained cells were analyzed using a FACS Aria III flow cytometer. Data were analyzed by Flow Jo software version 7.6 (FlowJo).

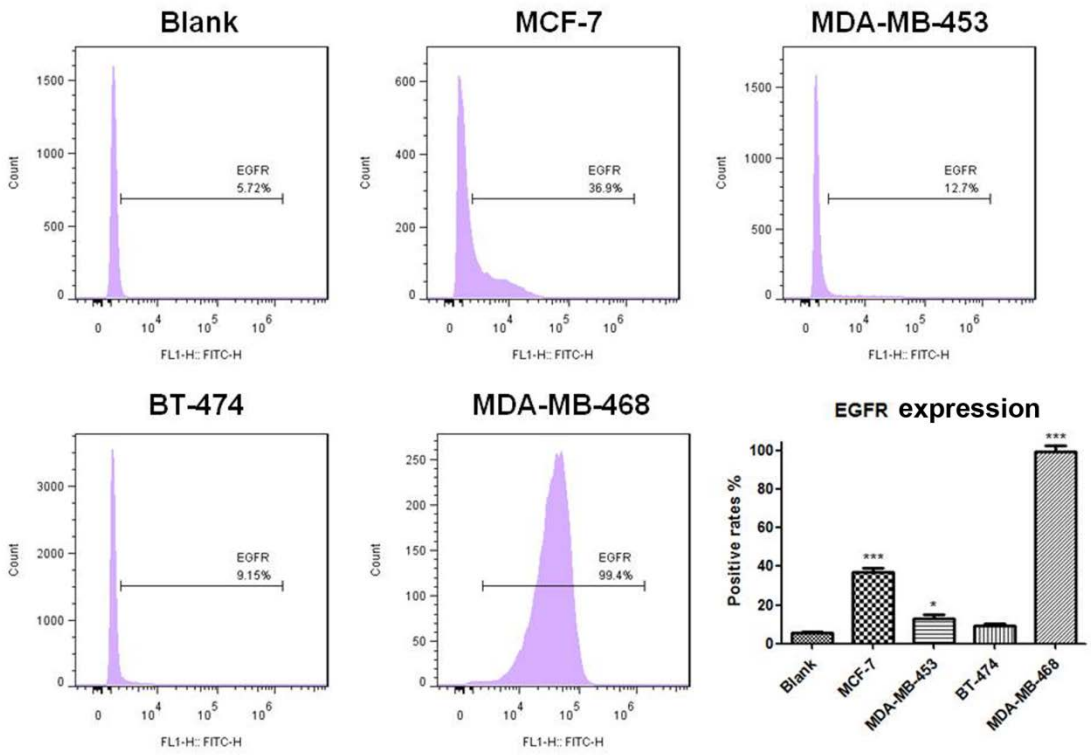

Supplemental Fig. 10. EGFR expression in different breast cancer cell lines measured by flow cytometry. (Compared with Blank group, *** $P < 0.001$)

Method: Human breast cancer cells (MCF-7, MDA-MB-453, BT-474, MDA-MB-468, 1×10^5 cells/mL) were collected, washed once with cold PBS, fixed with 4% paraformaldehyde (10 min) and then permeabilized with 0.1% PBS-Tween for 20 min. The cells were then incubated in 1x PBS/10% normal goat serum/0.3 M glycine to block non-specific protein-protein interactions followed by incubation with the antibody (ab134182, ab52894, Abcam) at 4 °C overnight. The secondary antibody Goat Anti-Rabbit IgG H&L (FITC) (ab97050, Abcam) was used with 1/100 dilution and incubated for 30 min at 22 °C. Stained cells were analyzed using a FACS Aria III flow cytometer. Data were analyzed by Flow Jo software version 7.6 (FlowJo).

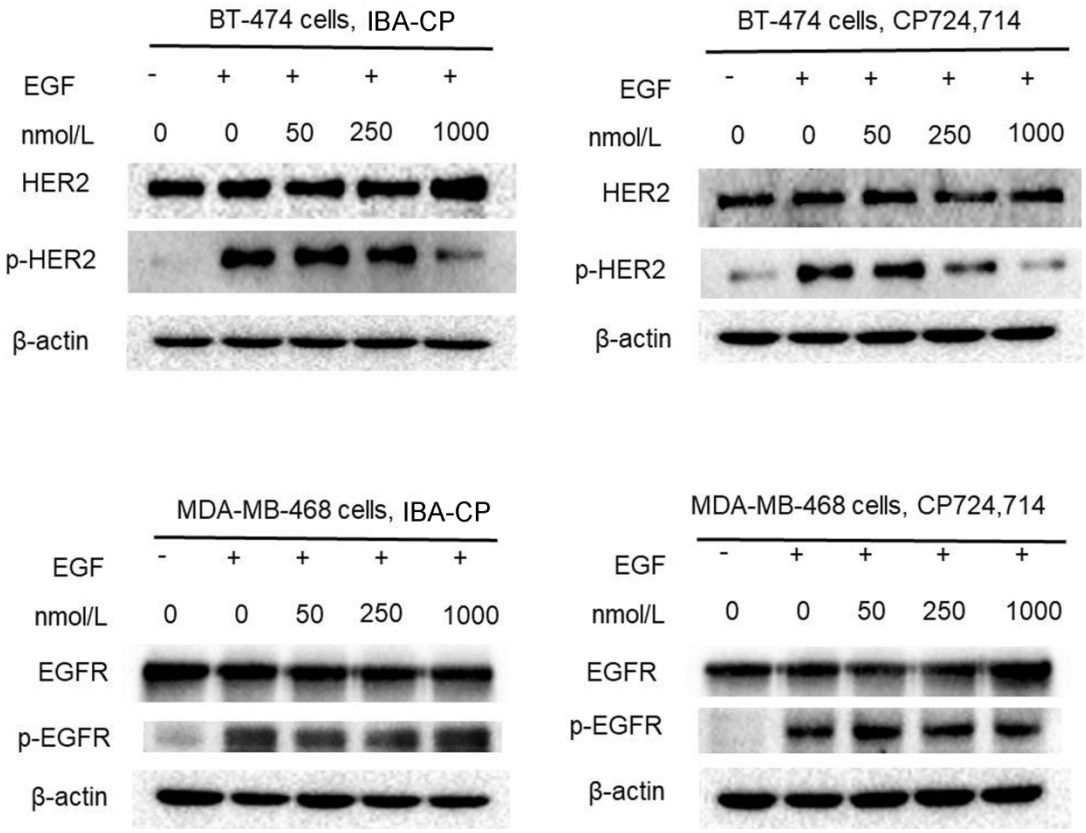

Supplemental Fig. 11. Western blot analysis of HER2, HER2 phosphorylation, EGFR and EGFR phosphorylation protein levels without or with different concentrations of IBA-CP or CP724,714 in BT-474 (HER2 +) and MD-MB-468 (EGFR +) cell lines.

Method: The cells were seeded in 6-well tissue culture plates at a density of 1 x 10^6 cells/well. After cell attachment, they were exposed to various concentrations of IBA-CP or CP-724,714 for 2 h. After incubation with the compound, appropriate wells were stimulated with 50 ng/mL EGF for 15 min or unstimulated (basal). After incubation, cells were lysed with RIPA Lysis (Thermo Scientific) on the ice, and total protein concentration was quantified using a BCA™ Protein Assay Kit (Pierce). Lysates were collected and boiled for 10 min. Equal amounts of total protein (20 µg) were loaded onto Bis-Tris gels for SDS-PAGE Western Blot electrophoresis and transferred to a polyvinylidene difluoride membrane. After transfer, membranes were blocked for 1 h at room temperature with 5% BSA in Tris-buffered saline (Sigma Chemical Co.), 0.1% Tween 20, then incubated overnight at 4°C with antibodies specific for HER2 (ab134182, Abcam), phospho-HER2 (2243S, Cell Signaling Technology); EGFR(ab52894, Abcam), phospho-EGFR (ab40815, Abcam), and β-actin (12262S, Cell Signaling Technology). The membranes were incubated with the antimouse or antirabbit HRP-conjugated secondary antibodies (31430, A27036, Thermo Scientific) for 1 h at room temperature. Proteins were visualized on a Bio-Rad ChemiDoc XRS System.

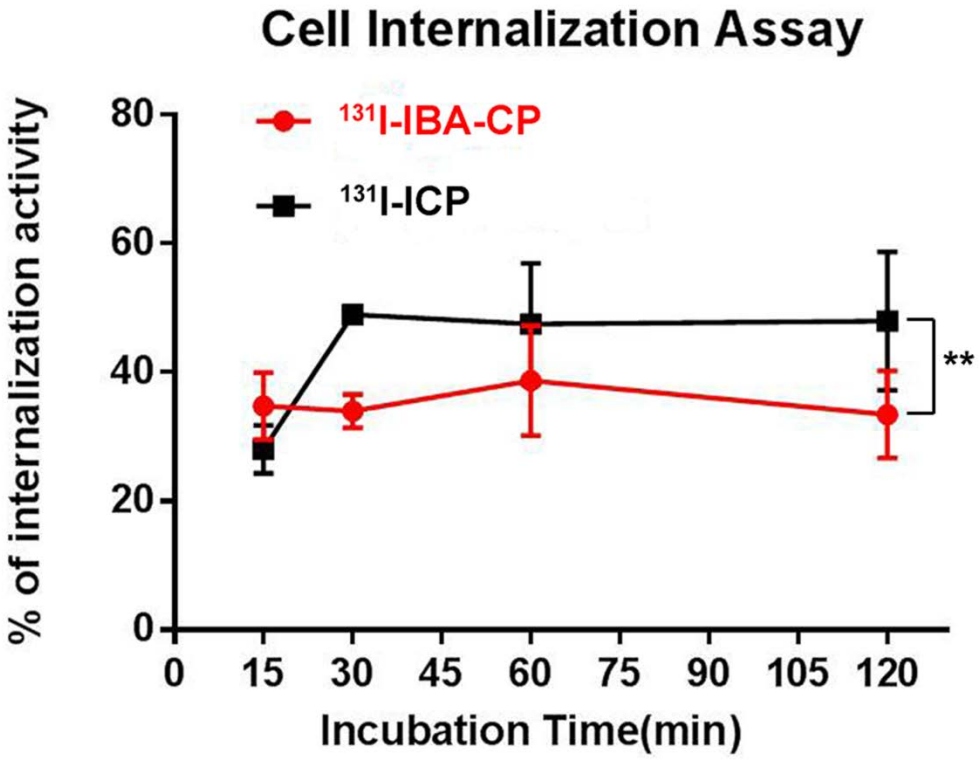

Supplemental Fig. 12. Cell internalization assay of ^{131}I-IBA-CP and ^{131}I-ICP in MDA-MB-453 cell line. Cell internalization assays of ^{131}I-IBA-CP and ^{131}I-ICP were conducted to compare their intracellular accumulation in MDA-MB-453 cells. Since ^{131}I-ICP is more lipophilic than ^{131}I-IBA-CP, it is reasonable that the amount of internalized ^{131}I-ICP is slightly more than that of ^{131}I-IBA-CP. (** $P < 0.05$)

Method: Cells were seeded in two 12-well plates (0.2 million/well) with culture medium and allowed to attach overnight. The cells were washed once with binding buffer (PBS, pH 7.4, plus 0.2% BSA), then 450 µL of binding buffer was added to each well. ^{131}I-IBA-CP or ^{131}I-ICP (25 µL, ~ 500,000 cpm/0.1 mL) was added to each well and incubated with MDA-MB-453 cells for 2 h at 4 °C. After pre-incubation, cells were washed with ice-cold binding buffer for three times, then incubated with previously warmed binding buffer for different time periods (15, 30, 60 and 120 min) at 37 °C. After that, the cells were incubated with acidic wash buffer (50 mM glycine-HCl/100 mM NaCl, pH 2.8) twice for 5 min at room temperature. Cells were solubilized by incubation with 1 N NaOH at 37 °C for 5 min, and radioactivity was measured with a well-type γ-counter.

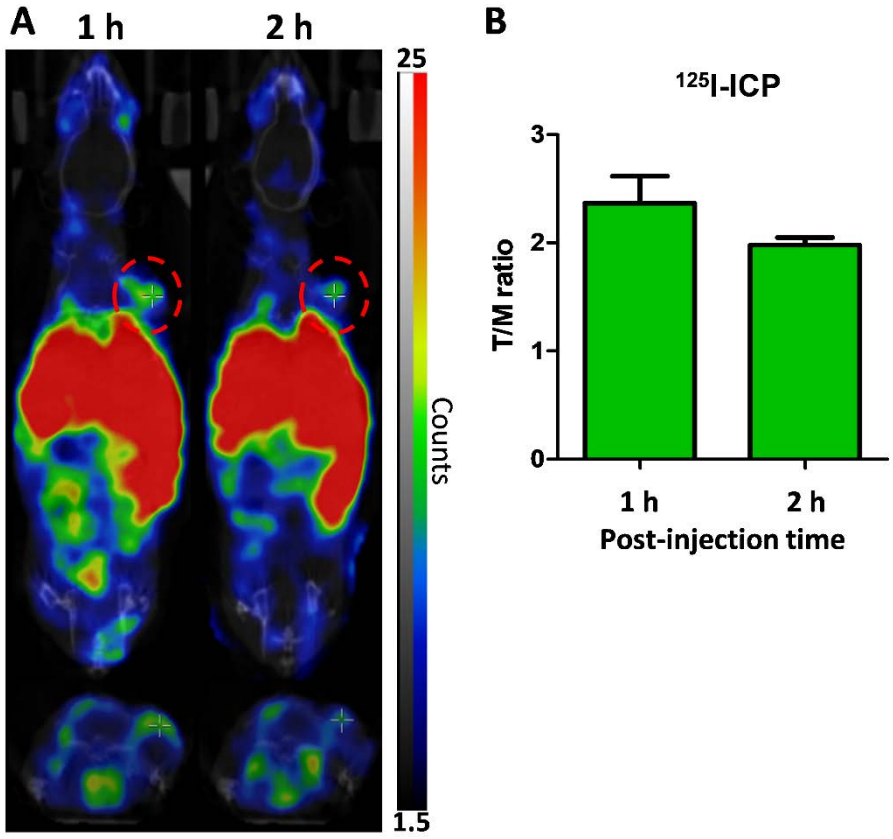

Supplemental Fig. 13. (A) Representative SPECT/CT images obtained at 1 h and 2 h after injection of ^{125}I-ICP in MDA-MB-453 (HER2+) tumor-bearing mice. The acquisition parameters were as follows: energy peak of 35 keV for ^{125}I, window width of 20%, matrix of 256 × 256, medium zoom, and frame: 30 s. All images were performed in the same manner and reconstructed, processed and further analyzed with Nucline software (Mediso Medical Imaging System) by drawing appropriate Volume of Interests on tumor and muscle; (B) Tumor to muscle activity ratios derived from SPECT imaging results.

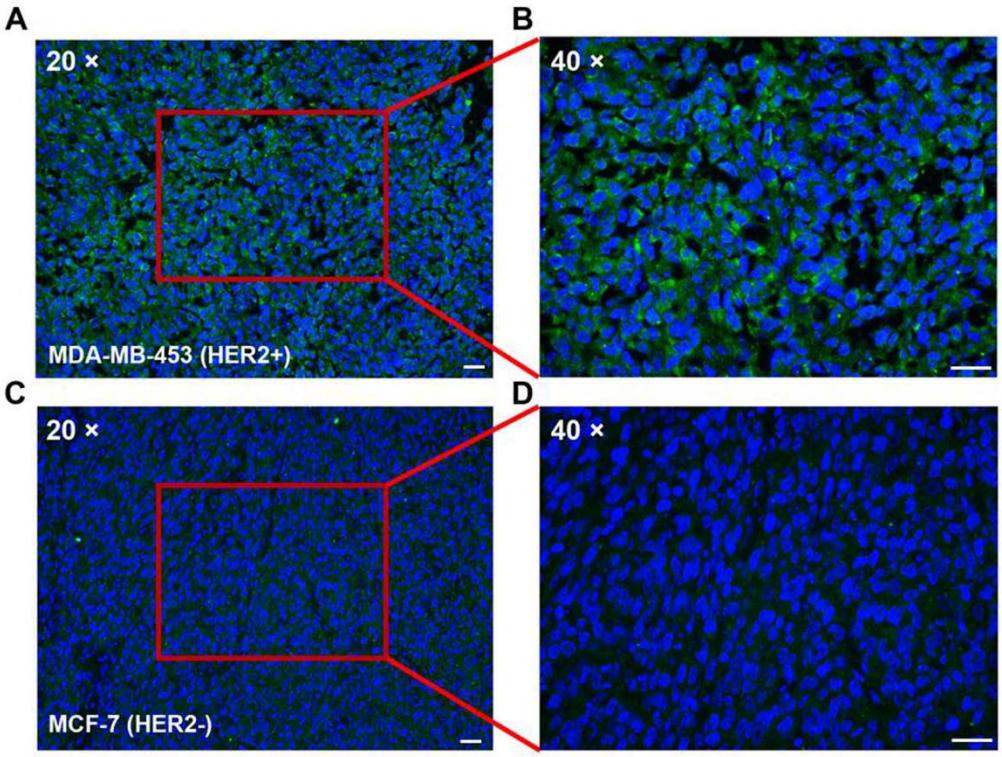

Supplemental Fig. 14. Microscope overview image of a region of MDA-MB-453 (HER2 positive) (A, B) and MCF-7 (HER2 negative) (C, D) tumor tissue sections labeled with DAPI (blue) and decorated with anti-HER2-FITC conjugate (green). Scale bar = 25 μm.

Method: After imaging, tumors were removed from the anesthetized mice. Formalin-fixed tumors (10%, v/v) were embedded in paraffin, coronally sectioned into 5-μm-thick slices, and mounted on microscope slides according to standard procedures (Histo-Tec Laboratory). Before staining, antigen retrieval was performed in 10 mM sodium citrate buffer at 90 °C for 10 min. The tissue sections were blocked with 10% donkey serum and labeled with the primary antibody against HER2 (anti-mouse, catalog number ab16901, Abcam, USA) in 5% goat serum (the species in which the secondary antibodies are raised) overnight. On the following day, tissues were labeled with FITC conjugated (green) secondary antibody (goat anti-Mouse IgG (H+L); catalog number A0568, Beyotime Biotechnology, China) for 1 h followed by washing in phosphate-buffered saline. The slides were mounted with VECTASHIELD Antifade Mounting Medium with 4', 6-diamidino-2-phenylindole (DAPI). Finally, the slides were evaluated under a microscope (200× and 400× amplification; Nikon).

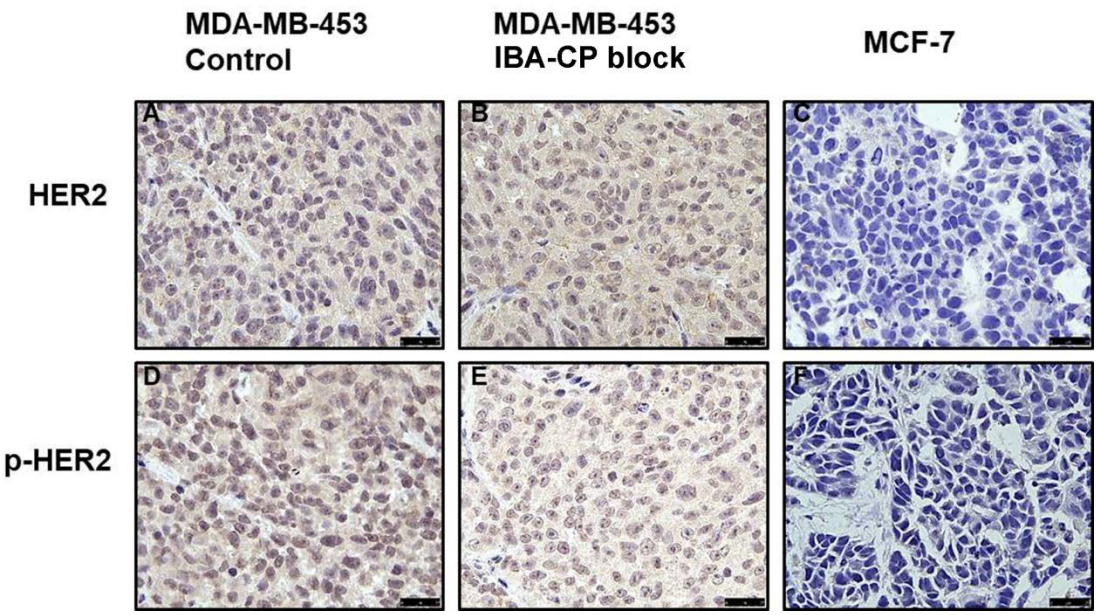

Supplemental Fig. 15. Representative IHC staining results for HER2, p-HER2 (original magnification 400 ×, scale bars, 25 μm).

Method: Tumor sections obtained from the blocking or control group mice were formaldehyde-fixed, paraffin-embedded and deparaffinized with xylene and rehydrated in decreasing concentrations of ethanol. After blocking endogenous peroxidase with 3% hydrogen peroxidase in methanol, sections were boiled in 0.01 M citrate buffer for 10 min and incubated with 5% normal blocking serum in Tris-buffered saline for 20 min. The sections were then incubated with the following antibodies: anti-human rabbit monoclonal antibodies against HER2, diluted 1:100, phospho-HER2, diluted 1:320, for 60 min at room temperature and followed by incubation with biotinylated goat anti-rabbit IgG (ab64256, Abcam). After incubation in an avidin-biotin-peroxidase complex for 30 min, the samples were exposed to diaminobenzidine tetrahydrochloride solution and counterstained with hematoxylin.

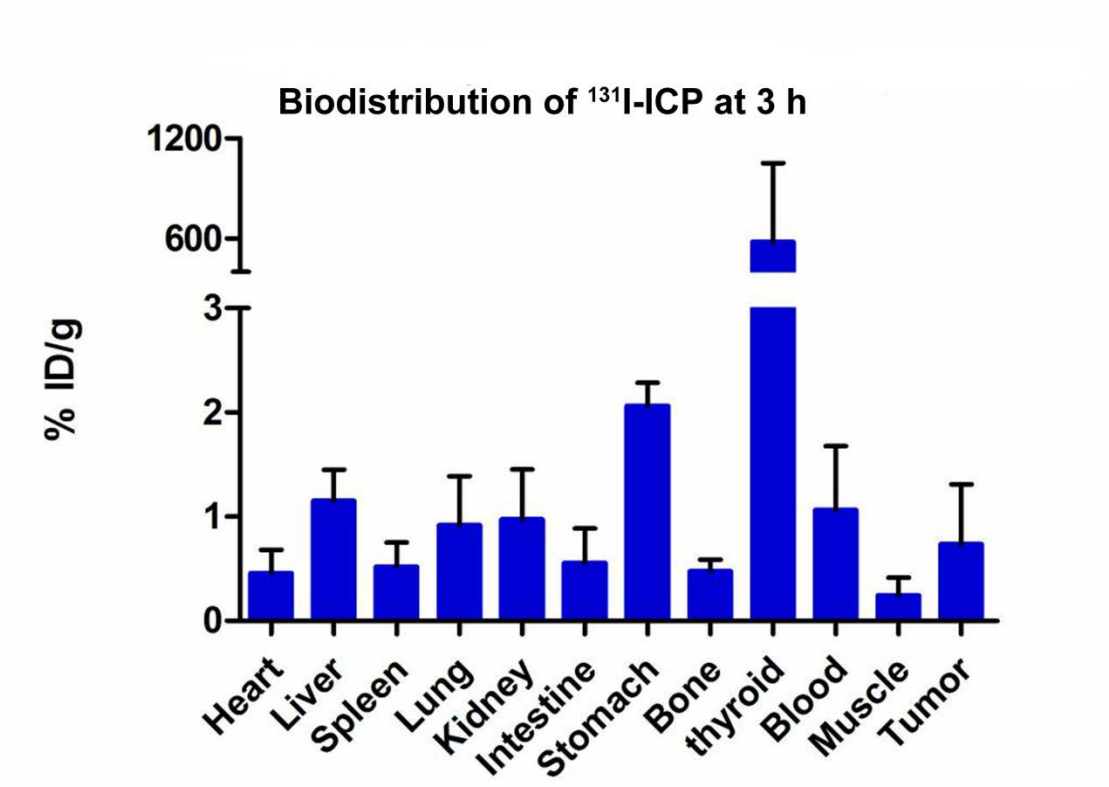

Supplemental Fig. 16. Biodistribution study of ^{131}I-ICP at 3 h after tracer injection in mice bearing MDA-MB-453 tumors. The distribution of ^{131}I-ICP in tumor and major organs (n = 4/group) were evaluated in female nude mice bearing MDA-MB-453 tumor xenograft by injection of 0.18 MBq ^{131}I-ICP. The mice were sacrificed and dissected at 3 h after injection. Samples of tumor, blood, liver (without the gallbladder) and other major organs were collected and weighed, and then the radioactivity in each sample was measured with a well-type γ-counter. To correct for radioactive decay and permit the calculation of radioactivity in each organ as a fraction of the administered dose, counts in aliquots of the injected doses were determined simultaneously. The results were expressed as mean ± SD of percentage injected dose per gram of sample (% ID/g).

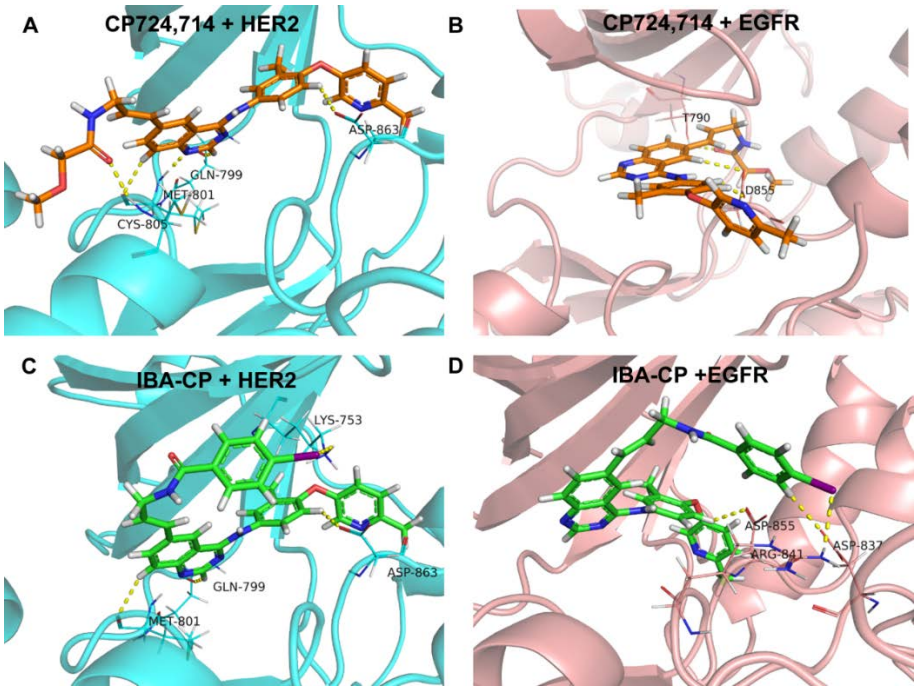

Supplemental Fig. 17. Docking poses of CP724,714 with HER2 (A) and EGFR (B), and IBA-CP with HER2 (C) and EGFR (D)

Method: We downloaded the crystal structures of EGFR (PDB ID code: 3POZ) and HER2 (PDB ID code: 3RCD), repaired the crystal structure by adding the missing side chains of residues and other missing atoms, and then removed all the crystal water molecules. The H-bonds were optimized using crystal symmetry and the crystal structure was minimized based on the converge heavy atoms to the default Root Mean Square Deviation (RMSD) value of 0.30 Å3 with an OPLS3 force field. The ligands, IBA-CP and CP724,714, were drawn with Maestro v10.1 (Schrödinger Release 2015-2: Glide, Schrödinger, LLC, New York, NY, 2015.) and possible states of the ligands at target pH 7.4 were generated with OPLS3 force field by Ligprep module. In the receptor grid generation step, a cubic box with 20 x 20 x 20 Å3 size was centered based on the mass center of the original co-crystal ligand O3P with a default parameter. Finally, all the different conformations of the ligands generated from the Ligprep were docked into the ATP-pocket of both kinase structures using Glide (Schrödinger Release 2015-2: Glide, Schrödinger, LLC, New York, NY, 2015.) with the standard default settings in standard precision mode. The best-scored pose of each ligand was selected for further study based on the GlideScore function, which was an empirical scoring function as shown below:

GlideScore = Hbond + Lipo + Metal + BuryP + RotB + Site + 0.065*vdW + 0.130*Coul

GlideScore comprised of terms that accounted for the physics of the binding process including a hydrogen bond term, lipophilic-lipophilic term, a rotatable bond penalty, and the term of protein-ligand coulomb-vdW energies (*5*).

REFERENCES

1. Kramer-Marek G, Kiesewetter DO, Martiniova L, Jagoda E, Lee SB, Capala J. [18F]FBEM-Z(HER2:342)-Affibody molecule-a new molecular tracer for in vivo monitoring of HER2 expression by positron emission tomography. *Eur J Nucl Med Mol Imaging.* 2008;35:1008-1018.

2. Barbacci EG, Pustilnik LR, Rossi AM, et al. The biological and biochemical effects of CP-654577, a selective erbB2 kinase inhibitor, on human breast cancer cells. *Cancer Res.* 2003;63:4450-4459.

3. Zhang P, Zhuang R, Guo Z, Su X, Chen X, Zhang X. A Highly Efficient Copper-Mediated Radioiodination Approach Using Aryl Boronic Acids. *Chem-Eur J.* 2016;22:16783-16786

4. Zhang X, Xiong Z, Wu Y, et al. Quantitative PET imaging of tumor integrin alphavbeta3 expression with 18F-FRGD2. *J Nucl Med.* 2006;47:113-121.

5. Friesner RA, Murphy RB, Repasky MP, et al. Extra precision glide: docking and scoring incorporating a model of hydrophobic enclosure for protein-ligand complexes. *J Med Chem.* 2006;49:6177-6196.